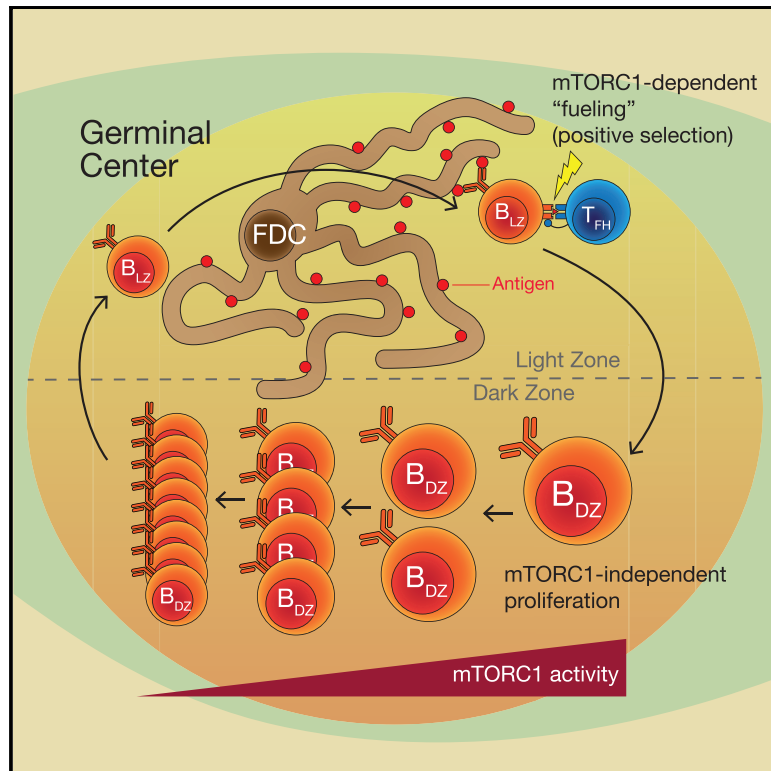# Immunity

Germinal Center Selection and Affinity Maturation Require Dynamic Regulation of mTORC1 Kinase

Graphical Abstract

Authors

Jonatan Ersching, Alejo Efeyan,
Luka Mesin, ..., David Dominguez-Sola,
David M. Sabatini, Gabriel D. Victora

Correspondence

victora@rockefeller.edu

In Brief

During germinal center selection, signals from Tfh cells in the light zone dictate the extent of B cell proliferation in the dark zone. Ersching et al. (2017) show that Tfh help induces mTORC1 activation in light zone B cells, leading to cell growth that sustains the subsequent dark zone proliferative burst.

Highlights

- Positive selection of GC B cells triggers mTORC1 activation prior to clonal expansion

- mTORC1 is required for biomass accumulation but dispensable for cell-cycle progression

- Deregulated mTORC1 promotes DZ phenotype and leads to loss of GC competitiveness

- Rapamycin-resistant mouse strain is used for cell-intrinsic mTORC1 inhibition

Data Resources

GSE98778

CrossMark

CellPress

Germinal Center Selection and Affinity Maturation Require Dynamic Regulation of mTORC1 Kinase

Jonatan Ersching,[1,6,9] Alejo Efeyan,[1,7,9] Luka Mesin,[1,6] Johanne T. Jacobsen,[1,2,6] Giulia Pasqual,[1,6] Brian C. Grabiner,[1,8] David Dominguez-Sola,[3] David M. Sabatini,[1,4,5] and Gabriel D. Victora[1,6,10,*]
[1]Whitehead Institute for Biomedical Research, Cambridge, MA, 02142, USA
[2]Center for Immune Regulation, Oslo University Hospital, University of Oslo, N-0372 Oslo, Norway
[3]Department of Oncological Sciences, The Tisch Cancer Institute and Graduate School of Biomedical Sciences, Icahn School of Medicine at Mount Sinai, New York, NY, 10029, USA
[4]Department of Biology, Massachusetts Institute of Technology, Cambridge, MA, 02142, USA
[5]Howard Hughes Medical Institute, Cambridge, MA, 02142, USA
[6]Present address, Laboratory of Lymphocyte Dynamics, The Rockefeller University, New York, NY 10065, USA
[7]Present address, Centro Nacional de Investigaciones Oncológicas, 28029, Madrid, Spain 10065, USA
[8]Present address, Biogen, Cambridge, MA, 02142, USA
[9]Equal contribution
[10]Lead contact
*Correspondence: victora@rockefeller.edu
http://dx.doi.org/10.1016/j.immuni.2017.06.005

SUMMARY

During antibody affinity maturation, germinal center (GC) B cells cycle between affinity-driven selection in the light zone (LZ) and proliferation and somatic hypermutation in the dark zone (DZ). Although selection of GC B cells is triggered by antigen-dependent signals delivered in the LZ, DZ proliferation occurs in the absence of such signals. We show that positive selection triggered by T cell help activates the mechanistic target of rapamycin complex 1 (mTORC1), which promotes the anabolic program that supports DZ proliferation. Blocking mTORC1 prior to growth prevented clonal expansion, whereas blockade after cells reached peak size had little to no effect. Conversely, constitutively active mTORC1 led to DZ enrichment but loss of competitiveness and impaired affinity maturation. Thus, mTORC1 activation is required for fueling B cells prior to DZ proliferation rather than for allowing cell-cycle progression itself and must be regulated dynamically during cyclic re-entry to ensure efficient affinity-based selection.

INTRODUCTION

Germinal centers (GCs) are the primary site of affinity maturation, the process whereby the affinity of serum antibodies increases with time after immunization (Eisen and Siskind, 1964). Affinity maturation relies on somatic mutation of immunoglobulin genes followed by positive selection—defined here as re-entry from light zone (LZ) to dark zone (DZ) followed by clonal expansion—of GC B cells that have attained improved affinity for antigen (Allen et al., 2007; MacLennan, 1994; Mesin et al., 2016; Victora and Nussenzweig, 2012). A key feature of this expansion is the ability of selected B cells to undergo sustained and rapid pro-

liferation in the DZ in the apparent absence of further antigen-dependent signals. This can be readily observed when selection is artificially induced by forcing GC B cell-T follicular helper (Tfh) cell interactions (Gitlin et al., 2015; Gitlin et al., 2014; Victora et al., 2010), but is also likely to be at the origin of the "clonal bursts" that can lead to radical loss of clonal diversity in GCs under unmanipulated conditions (Tas et al., 2016). The finding that the number of B cell divisions in the DZ is proportional to the strength of the signals from Tfh cells in the LZ (Gitlin et al., 2014) suggests the existence of B cell-intrinsic molecular circuits that link positive selection in the LZ to sustained DZ proliferation and determine the timing of the return of these cells to the LZ (Bannard et al., 2013). Previous work by us and others has shown that c-Myc, a key regulator of cell cycle and the driver oncogene in Burkitt lymphoma, is induced in GC B cells upon positive selection in the LZ (Calado et al., 2012; Dominguez-Sola et al., 2012) and that its activity is prolonged upon migration of selected cells to the DZ by c-Myc-dependent induction of the related transcription factor AP4 (Chou et al., 2016). However, c-Myc expression alone is insufficient to drive a robust proliferative program in B cells (Sander et al., 2012), and therefore additional pathways are likely required to link positive selection in the LZ to sustained cell cycling in the DZ.

The mechanistic target of rapamycin (mTOR) is a serine-threonine kinase critically involved in the control of anabolism and metabolic reprogramming in immune cells (Powell et al., 2012). A range of stimuli—including energy, amino acids, oxygen, glucose, growth factors, and immune signals—activate mTOR complex 1 (mTORC1), which in turn activates multiple anabolic programs that lead to cell growth (Laplante and Sabatini, 2012). In the immune system, mTORC1 has been linked to T cell differentiation, tolerance, anergy, and migration (Araki et al., 2009; Sinclair et al., 2008; Zeng et al., 2013; Zheng et al., 2007), as well as to B cell differentiation and antibody production (Jones et al., 2016; Limon et al., 2014; Lin et al., 2015; Omori et al., 2006). However, fine dissection of the specific role of mTORC1 in GC selection has been difficult to achieve, because genetic or pharmacological inhibition of this pathway in mice

CrossMark

normally leads to GC dissolution (Jones et al., 2016; Keating et al., 2013; Zhang et al., 2013). Given that GC B cells cycle asynchronously between proliferation in the DZ and selection in the LZ, such approaches do not allow for an analysis of the specific requirements for mTORC1 at different stages of positive selection.

Here, we have used an in vivo model to target and synchronize positive selection to a predefined subset of GC B cells, which allowed us to investigate the specific role of mTORC1 in this process in a time-resolved manner. We found that mTORC1 activation was required early after positive selection to trigger the anabolic cell growth that sustained extensive cell division in the DZ, but became largely dispensable once this proliferative program had been initiated. We thus propose a model in which GC B cell anabolism triggered by mTORC1 links the strength of antigen-dependent selection in the LZ to the extent of clonal expansion in the DZ.

RESULTS

Positive Selection of GC B Cells Activates mTORC1 in a CD40-Dependent Manner

To investigate the molecular pathways associated with GC positive selection in vivo, we used a previously developed protocol in which selection of a traceable subpopulation of GC B cells can be triggered by targeted delivery of antigen via the surface lectin DEC-205 (encoded by the gene $Ly75$). This protocol forces targeted GC B cells to interact with Tfh cells, triggering LZ to DZ migration and extensive cell proliferation (Victora et al., 2010); positive selection then proceeds in a synchronous manner, and can be followed over time. In brief, we co-transfer into oval-bumin (OVA)-primed recipient mice two populations of naive B cells, a majority population (85%) that is deficient for DEC-205 ($Ly75^{-/-}$) (Inaba et al., 1995) and a minority population (15%) which is $Ly75^{+/+}$ (Figure 1A). Both $Ly75^{+/+}$ and $Ly75^{-/-}$ populations express a B1-8^{hi} variant of the Ig heavy chain that, when paired to an Igλ light chain, bind with high affinity to 4-hydroxy-3-nitro-phenylacetyl (NP) (Shih et al., 2002). Boosting with NP-OVA generates GCs that contain B1-8^{hi} B cells at a proportion similar to that of the input population (85% $Ly75^{-/-}$/15% $Ly75^{+/+}$), which are helped by OVA-specific Tfh cells. Subsequent injection of an antibody to DEC-205 recombinantly fused to OVA (DEC-OVA) ensures delivery of the T cell antigen to $Ly75^{+/+}$ GC B cells only, strongly skewing T cell help toward these cells and triggering positive selection (Victora et al., 2010).

To determine which transcriptional programs are induced by positive selection in this model, we isolated and sequenced mRNA from $Ly75^{+/+}$ and $Ly75^{-/-}$ LZ B cells 12 hr after DEC-OVA injection, a time point when $Ly75^{+/+}$ cells were enriched in the LZ, strongly interacting with Tfh cells (Shulman et al., 2014). As expected from our previous findings (Dominguez-Sola et al., 2012), Gene Set Enrichment Analysis (GSEA) (Subramanian et al., 2005) revealed strong upregulation of gene signatures associated with the cellular response to c-Myc (Schuhmacher et al., 2001; Sun et al., 2017; Zeller et al., 2003) (Figure S1A). Of note, comparison with our own previously published signature of genes upregulated in GC B cells expressing c-Myc, which marks B cells currently undergoing positive selection under steady state (Dominguez-Sola et al., 2012), showed substantial

coincidence between the two programs (Figure S1B), further supporting the notion that Tfh cells are bona fide drivers of GC positive selection.

GSEA analysis also showed strong upregulation in $Ly75^{+/+}$ B cells of signatures related to the activation of mTORC1 (Figure 1B). These included genes downregulated in a human B cell lymphoma line (BJAB) by treatment with the mTORC1 inhibitor rapamycin or by removal of leucine from tissue culture media (which also inhibits mTORC1) (Peng et al., 2002). Thus, in addition to c-Myc, GC positive selection also appears to involve activation of mTORC1. To verify this directly, we immunized mice with NP conjugated to keyhole limpet hemocyanin (KLH) in alum and stained histological sections of draining lymph nodes 14 days later for the phosphorylation of ribosomal protein S6 on serines 235 and 236 (targets of S6 kinase, itself a target of mTORC1). Although most GC cells showed increased S6 phosphorylation when compared to naive B cells, cells with the highest amounts of phospho-S6 were detected predominantly in the LZ, with marked enrichment among c-Myc-expressing cells (Figures 1C and S1C). This enrichment was confirmed by flow cytometry using a reporter mouse strain carrying a GFP-Myc fusion protein (Huang et al., 2008) (Figure 1D). Thus, mTORC1 activity is upregulated specifically in LZ cells during positive selection and concomitantly with activation of c-Myc.

To investigate the kinetics of mTORC1 induction, we forced B cell-Tfh cell interaction with DEC-OVA as in Figure 1A and measured the extent of S6 phosphorylation over time (Figures 1E and 1F). DEC-OVA induced robust phosphorylation of S6 as early as 12 hr post-treatment, when targeted cells are found predominantly in the LZ interacting with Tfh cells (Shulman et al., 2014). Increased phosphorylation persisted up to at least 36 hr after DEC-OVA, by which time most selected cells have already migrated to the DZ (Victora et al., 2010), and returned to steady-state by 72 hr post-treatment. Phosphorylation of S6 protein was less pronounced when mice were given a lower dose of DEC-OVA or when the proportion of $Ly75^{+/+}$ B cells was increased (which increases competition among $Ly75^{+/+}$ B cells for Tfh cell help) (Figures 1G and 1H). Thus, GC B cells respond dynamically to the availability of T cell help by activating the mTORC1 pathway to different degrees. Mechanistically, injection of an antagonist antibody to CD40L (MR-1) prior to DEC-OVA fully prevented the increase in S6 phosphorylation (Figures 1I and 1J), and conversely, treatment of mice bearing GCs induced by immunization with KLH in alum with a CD40 agonist antibody (FGK4.5) induced strong S6 phosphorylation in GC B cells (Figures S1D and S1E). Thus, CD40 ligation is both necessary and sufficient for activation of the mTORC1 pathway in GC B cells during positive selection. We conclude that CD40-mediated interaction with Tfh cells leads to dose-dependent activation of the mTORC1 pathway in LZ B cells, which then decreases progressively as these cells migrate to the DZ and undergo multiple rounds of proliferation.

mTORC1 Activation in Positively Selected GC B Cells Promotes Ribosome Biogenesis and Cell Growth
The best-characterized role of mTORC1 is to drive cellular growth by inducing anabolism and ribosomal biogenesis (Laplante and Sabatini, 2012). Accordingly, $Ly75^{+/+}$ GC B cells showed increases in in vivo glucose uptake, (ds)RNA content
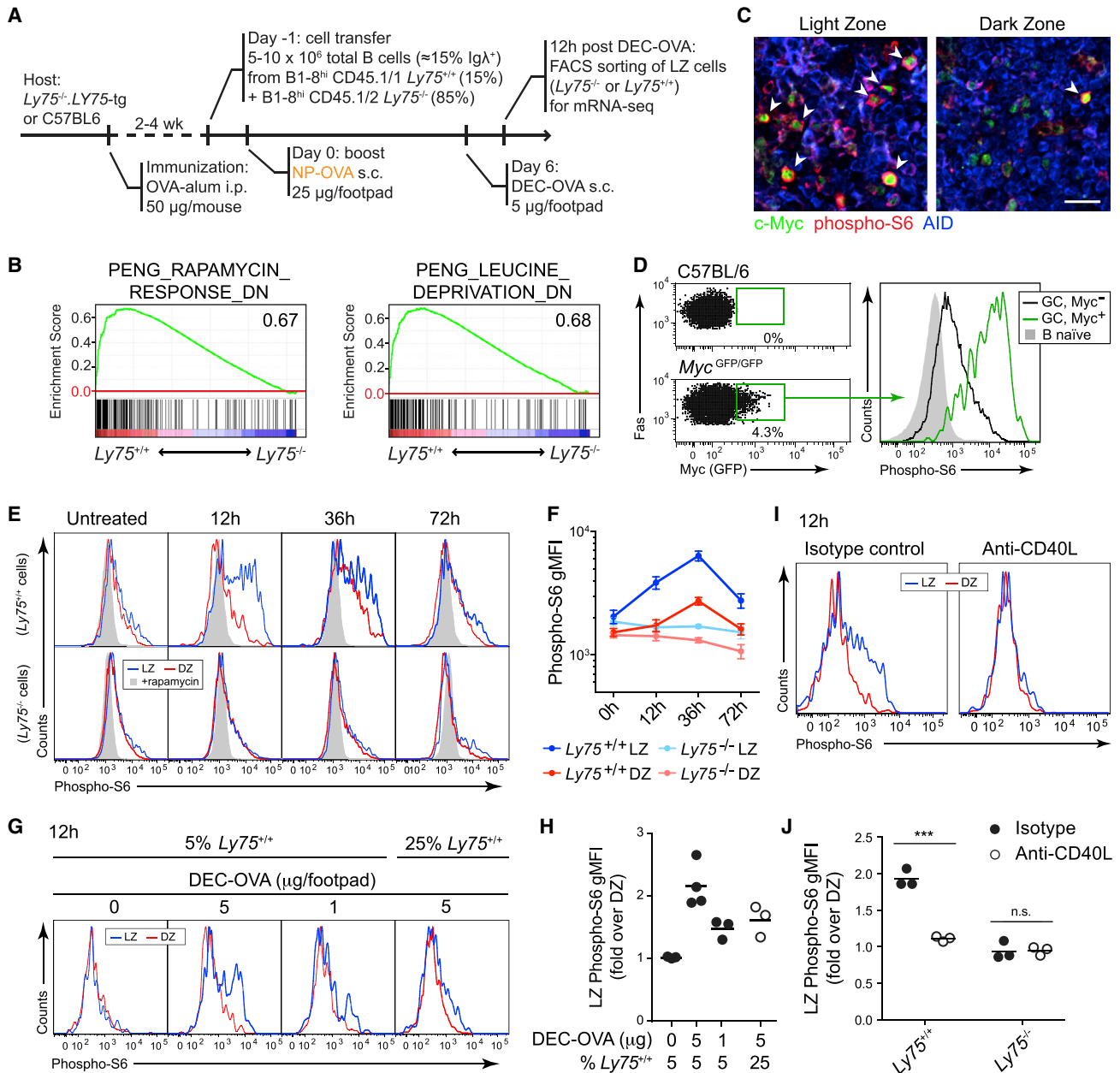
Figure 1. GC B Cells Activate mTORC1 upon Positive Selection

(A) Experimental setup for RNA-seq of $Ly75^{+/+}$ GC B cells following forced positive selection using DEC-OVA. Host mice were $Ly75^{-/-}.LY75$-tg in (B), (E), and (F) and wild-type C57BL6 in (G)–(J) (see STAR Methods).

(B) Enrichment of gene signatures related to activation of the mTORC1 pathway in LZ $Ly75^{+/+}$ GC B cells 12 hr after DEC-OVA injection. Number in top-right corner is the enrichment score; all p values and FDRs = 0 (below detection).

(C) Immunofluorescence showing c-Myc and phospho-S6 in LZ and DZ cells from popliteal lymph node GCs 14 days after footpad immunization with NP-KLH in alum. Scale bar represents 50 μm.

(D) Phospho-S6 staining in c-Myc-positive and negative GC B cells from popliteal lymph nodes of $Myc^{GFP/GFP}$ reporter mice 12 days after footpad immunization with KLH in alum. GFP fluorescence in GC B cells from a wild-type C57BL6 is shown as a control.

(E and F) Phospho-S6 staining in LZ and DZ cells at the indicated time points after DEC-OVA-targeted positive selection of $Ly75^{+/+}$ GC B cells, following the setup depicted in (A).

(G and H) Phospho-S6 staining in $Ly75^{+/+}$ GC B cells after positive selection using different doses of DEC-OVA or at different proportions of $Ly75^{+/+}$ B1-8^{hi} B cells in the adoptive transfer (5% versus 25%).

(I and J) Phospho-S6 staining in $Ly75^{+/+}$ GC B cells following blockade of CD40L. Mice were injected intravenously with 200 μg of a blocking antibody to CD40L (clone MR-1) or a matched isotype control 2 hr prior to DEC-OVA. Samples in panels (G–J) were analyzed 12 hr after DEC-OVA. ***p < 0.001, n.s., non-significant unpaired Student's t test. Bars indicate mean ± SEM. All data are from at least two independent experiments. (B, n = 3; C, n = 3; D, n = 4; E and F, n = 5–6; G and H, n = 3–4; I and J, n = 3) See also Figure S1.

(which consists mostly of ribosomal RNA), and forward scatter (FSC, a surrogate for cell size) in response to DEC-OVA, all of which were at least partly abrogated by treatment with rapamycin (Figures 2A–2D). Detailed kinetic analysis (Figures 2E–2H and S2) showed that FSC and dsRNA content peak simultaneously at 36 hr after DEC-OVA treatment, which roughly coincided with the onset of the proliferative burst that positively selected cells undergo in the DZ (shaded area in Figures 2E–2H). Concomitant measurement of S6 phosphorylation showed that the rise in mTORC1 activity preceded the increase in FSC and dsRNA content by approximately 12 hr, consistent with a role for mTORC1 in driving GC B cell growth prior to proliferation. All three parameters decreased during the strong proliferative phase in which the $Ly75^{+/+}$ cell population rapidly expanded in the DZ (shaded gray area in Figures 2E–2H), returning to baseline as these cells reentered the LZ between 72 and 96 hr post-treatment (Figure 2H). Thus, mTORC1 activation triggers an anabolic program that involves increased glucose uptake, ribosomal biogenesis, and cell growth in positively selected B cells. Of note, the peak of this program preceded, rather than being concomitant with, the proliferative burst that takes place subsequently in the DZ.

The coincidence in time between the decrease in cell size and return to steady-state DZ/LZ ratio (Figure 2E and 2H) led us to hypothesize that the timing of the return to the LZ after the DZ proliferative phase may be related to loss of cellular biomass. This predicts that positively selected B cells returning from DZ to LZ would be on average smaller than those being retained in the DZ. To test this, we triggered positive selection with DEC-OVA using B1-8^{hi} cells that express a photoactivatable (PA)-GFP transgene (Victora et al., 2010), and can thus be photolabeled in vivo based on their anatomical position (Figure 3A). At 48 hr after DEC-OVA, when most positively selected cells are large and actively proliferating in the DZ (where they remain for approximately another 24–48 hr), we photoactivated PA-GFP$^+$ cells in the DZ and then analyzed lymph nodes by flow cytometry 8 hr later. This strategy allowed us to identify "early emigrant" B cells, which left the DZ for the LZ (and acquired LZ surface markers) earlier than expected (Figures 3B and 3C). Early emigrants thus identified were on average smaller than the cells that remained in the DZ over this 8 hr period and were more similar in size to the counterselected $Ly75^{-/-}$ cells from the same LN (dotted lines in Figure 3D). Thus, the end of the proliferative phase that positively selected GC B cells undergo in the DZ correlates with smaller cell size, thus linking return from DZ to LZ to the anabolic state of the cell.

mTORC1 Is Required for LZ to DZ Migration and Cell Growth Prior to Clonal Expansion, But Not for Cell Cycle Progression

Our kinetic data suggested a scenario in which mTORC1 allows selected LZ cells to reach the size and anabolic capacity necessary to sustain multiple division cycles in the DZ (Figure 2 and 4A). This hypothesis predicts that selected cells would require mTORC1 activity only during the period of growth preceding the proliferative burst, but that active mTORC1 would be dispensable after the cells have reached peak size. To test this, we inhibited mTORC1 activity by injection of rapamycin 12, 24, or 36 hr after forcing positive selection of $Ly75^{+/+}$ cells with DEC-OVA (Figures 4A and 4B). These time points corre-

spond to suppressing mTORC1 before (12 hr), midway through (24 hr), and after (36 hr) the period of cell growth, but in all cases before any substantial proliferation has taken place. Lymph nodes were harvested and analyzed by flow cytometry at 48 hr after DEC-OVA treatment. Treatment with rapamycin at 12, 24, and 36 hr after DEC-OVA injection equally suppressed phosphorylation of S6 (Figures S3A and S3B), but it only effectively prevented the expansion of the $Ly75^{+/+}$ cells when administered 12 hr after DEC-OVA (Figure 4C). Notably, rapamycin had little effect on subsequent cell proliferation when injected after the culmination of the growth phase at 36 hr after DEC-OVA treatment, even when cells were analyzed at 60 hr after DEC-OVA (24 hr post-rapamycin) (Figures 4D). Even more pronounced was the effect of rapamycin on the ability of positively selected LZ B cells to transition to and maintain a DZ program (Figures 4E and 4F). Again, this effect was especially strong when rapamycin was administered 12 hr after DEC-OVA, but was still noticeable when the drug was administered at 36 hr, a point at which most LZ to DZ transition has already occurred. LZ entrapment of GC B cells upon rapamycin treatment was associated with failure to upregulate Foxo1, an essential regulator of the DZ phenotype (Dominguez-Sola et al., 2015; Sander et al., 2015) (Figure 4G).

Despite its effect on clonal expansion when administered prior to cell growth, flow cytometric measurement of DNA content (Figures 4H and 4I) and rate of S phase entry (Gitlin et al., 2014) (Figure 4J) showed that rapamycin treatment did not cause cell cycle arrest in $Ly75^{+/+}$ B cells, irrespective of time of administration. Consistent with these observations, global gene expression analysis showed that rapamycin had only a mild effect on the ability of DEC-OVA to drive the upregulation of gene signatures associated with c-Myc and its proliferative program, although it strongly suppressed upregulation of mTORC1-related signatures (Figure S3C). Similarly, treatment with rapamycin only slightly decreased the expression of GFP-c-Myc in steady-state GC B cells (Figure S3D). Thus, the effects of rapamycin are unlikely to be fully explained by functional cross-talk between mTORC1 and c-Myc. Overall, we conclude that the essential roles of the rapamycin-sensitive arm of the mTORC1 pathway in GC selection are to trigger the anabolic program that precedes proliferation and to regulate LZ to DZ positioning, rather than to directly regulate cell-cycle progression.

Unlike traditional genetic ablation approaches, using rapamycin to probe the function of mTORC1 in vivo allows tight kinetic regulation, which is crucial when dealing with highly dynamic reactions such as the GC. A key caveat to the use of chemical inhibitors in vivo, however, is the lack of cellular specificity—that is, systemic administration of rapamycin will presumably inhibit mTORC1 function throughout the organism, and therefore direct effects on B cells cannot be discerned from indirect effects via other cell types. To address this, we developed a chemical-genetic approach to target rapamycin resistance specifically to GC B cells in vivo. We used CRISPR/Cas9 genomic editing in zygotes (Wang et al., 2013; Yang et al., 2013a) to introduce a point mutation into exon 45 of the *Mtor* gene (F2108L) that confers resistance to rapamycin (Figures 5A and S4A and S4B). This mutation, identified in a human thyroid cancer resistant to Everolimus (a rapamycin analog), confers drug resistance in a dominant fashion by preventing the docking of the rapamycin-FKBP12
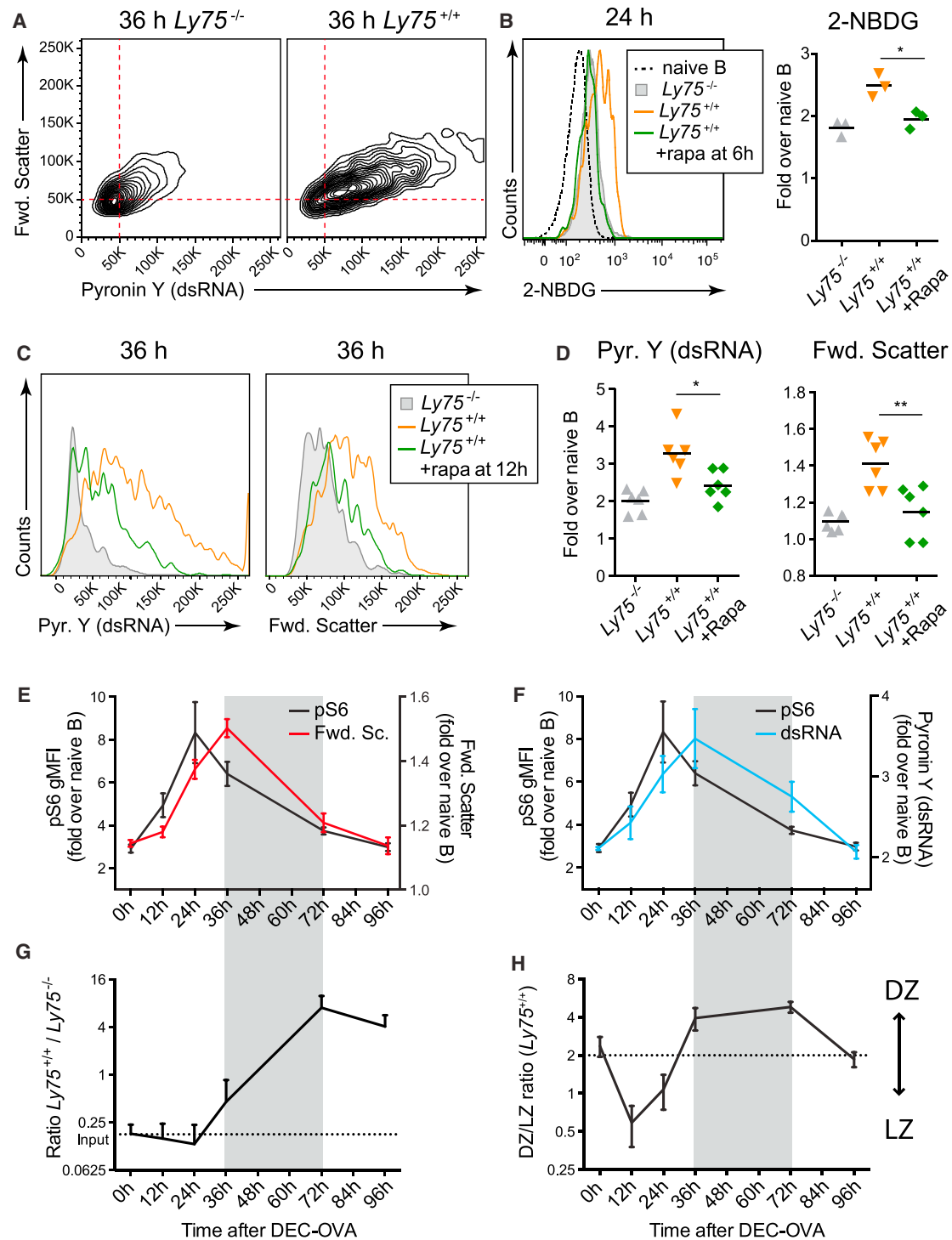
Figure 2. mTORC1 Activation in GC B Cells Leads to Ribosomal Biogenesis and Cell Growth

(A) Forward scatter and Pyronin Y staining (dsRNA content) in $Ly75^{+/+}$ and $Ly75^{-/-}$ GC B cells 36 hr after DEC-OVA injection.

(B) Glucose uptake in vivo by $Ly75^{+/+}$ and $Ly75^{-/-}$ GC B cells, 24 hr after DEC-OVA injection, with or without injection of rapamycin at 6 hr after DEC-OVA. Measured by intravenous injection of 5 mg/kg of 2-(N-(7-nitrobenz-2-oxa-1,3-diazol-4-yl)amino)-2-deoxyglucose (2-NBDG) 25 min prior to organ harvesting.

(C and D) Pyronin Y staining and forward scatter of $Ly75^{+/+}$ cells 36 hr after DEC-OVA injection, with or without treatment with rapamycin 12 hr after DEC-OVA.

(E–H) Kinetics of forward scatter, S6 phosphorylation, Pyronin Y staining, expansion of $Ly75^{+/+}$ cells ($Ly75^{+/+}/Ly75^{-/-}$ ratio) and $Ly75^{+/+}$ DZ/LZ ratio following DEC-OVA injection. *p < 0.05, **p < 0.01, unpaired Student's t test. Bars indicate mean ± SD. Data pooled from at least two independent experiments. (A, n = 6; B, n = 3; C and D, n = 6; E–H, n = 4–7). See also Figure S2.
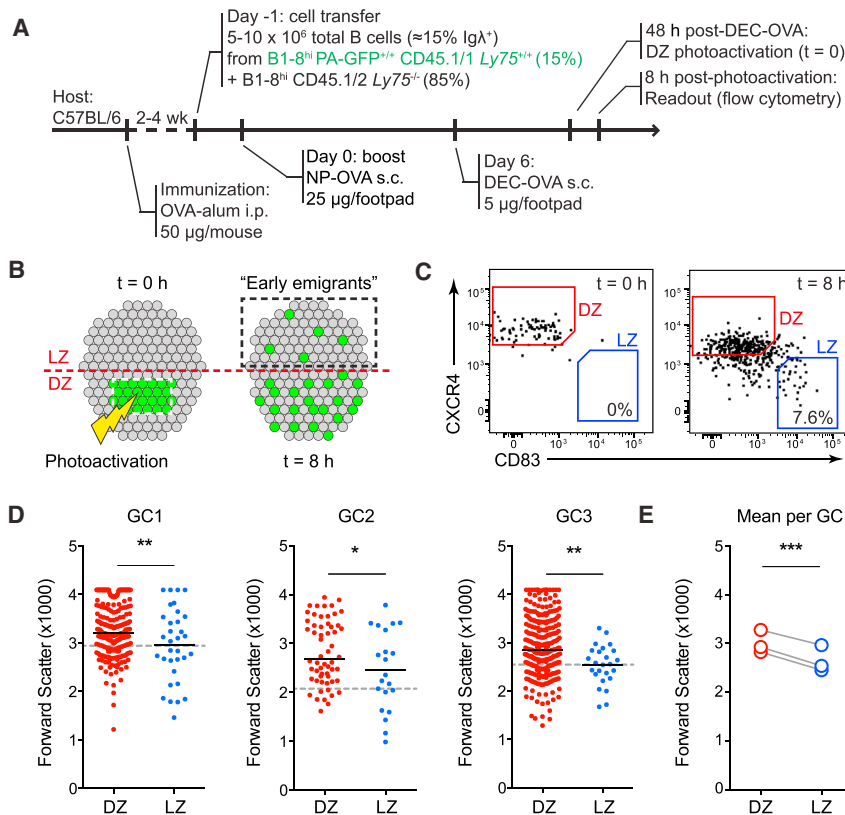
Figure 3. Decreased Cell Size Correlates with Return from DZ to LZ

(A and B) Experimental setup for assessment of migration of early DZ to LZ emigrants by flow cytometry.

(C) Representative plots showing photoactivated cells in DZ (red gates) and LZ (blue gates) at 0 hr or 8 hr after photoactivation.

(D) Forward scatter of individual cells in DZ and LZ 8 hr after photoactivation of single GCs. Dashed lines indicate the average cell size of $Ly75^{-/-}$ GC B cells from the same GC. Bars indicate mean.

(E) DZ and LZ cell size average from each GC. *p < 0.05, **p < 0.01, ***p < 0.001, unpaired Student t test. Each GC is from a different mouse in three independent experiments (n = 3).

$Mtor^{F2108L}$ allele rescued the effects of rapamycin on all of these parameters (Figures 5I and 5J and S5G). Of note, although rapamycin inhibited S6 phosphorylation in Tfh cells in $Mtor^{+/+}$ hosts but not in $Mtor^{F2108L/F2108L}$ hosts (Figure 5K), the effectiveness of rapamycin depended exclusively on the genotype of the transferred GC B cells. Thus, although mTORC1 plays a clear role in Tfh cell differentiation (Zeng et al., 2016), our results suggest that inhibiting this pathway in mature Tfh cells has little measurable effect

complex to mTOR (Wagle et al., 2014). Accordingly, cultured tail fibroblasts from the $Mtor^{F2108L/+}$ founder mouse were resistant to rapamycin treatment in vitro (Figure 5B). To test resistance in vivo, we triggered mTORC1 activation by fasting and then refeeding mice in the presence or absence of rapamycin (Efeyan et al., 2014). While rapamycin abrogated feeding-induced phosphorylation of mTORC1 targets in liver and cardiac and skeletal (gastrocnemius) muscles of $Mtor^{+/+}$ mice, liver, and cardiac muscle of $Mtor^{F2108L/+}$ mice were fully resistant to the drug, with the gastrocnemius muscle showing partial resistance (Figures S4C–S4E). Of note, the $Mtor^{F2108L}$ allele behaved as a mildly hypomorphic allele in gastrocnemius muscle but not in cardiac muscle or liver, correlating with the intrinsic mTORC1 activity in each organ.

To address the cell-specific effect of rapamycin in GC B cells, we performed experiments analogous to those described in Figure 4 but in which rapamycin-sensitive ($Mtor^{+/+}$) B1-8^{hi} B cells were transferred into rapamycin-resistant ($Mtor^{F2108L/F2108L}$) hosts (Figures 5C and S5A). As expected, rapamycin treatment led to robust loss of DEC-OVA-induced S6 phosphorylation in the transferred B1-8^{hi} GC B cells, but not in the minor population of host-derived B cells also present in B1-8^{hi} GCs (Figures 5D and S5B and S5C). As with wild-type hosts (Figures 2 and 4), rapamycin prevented DEC-OVA driven B1-8^{hi} cell growth (Figure S5D), clonal expansion (Figure 5E), and accumulation in the DZ (Figure 5F), consistent with a B cell-intrinsic requirement for mTORC1. Conversely, when selection of rapamycin-resistant $Ly75^{+/+}$ B1-8^{hi} B cells was forced within rapamycin-sensitive hosts (Figures 5G and 5H and S5E and S5F), presence of the

on their short-term ability to promote GC B cell selection. We conclude that GC B cell growth, proliferative expansion, and LZ to DZ transition require cell-intrinsic activity of mTORC1.

Deregulated mTORC1 Activation Decreases GC B Cell Competitiveness and Impairs Affinity Maturation

We next sought to determine whether mTORC1 activation alone is sufficient to favor positive selection of GC B cells, or whether, conversely, constitutively high mTORC1 activity has an adverse effect on GC B cell competitiveness. To this end, we generated a gain-of-function model in which mice bearing a loxP-flanked allele of the mTORC1 inhibitor $Tsc1$ (Kwiatkowski et al., 2002) were crossed to strains expressing Cre recombinase from the $Aicda$ (AID) locus (Robbiani et al., 2009) and to the genetically targeted B1-8^{hi} Igh allele. Cre-driven recombination in this model leads to strong constitutive mTORC1 activity in GC B cells specifically. We adoptively transferred a 1:1 mixture of $Aicda^{cre/+}.Tsc1^{fl/fl}$ B1-8^{hi} and $Aicda^{cre/+}.Tsc1^{+/+}$ B1-8^{hi} B cells into WT hosts, which we then immunized with NP-OVA (Figure 6A). As expected, GC B cells on the $Aicda^{cre/+}.Tsc1^{fl/fl}$ background showed strong mTORC1 activation, as determined by S6 phosphorylation (Figure 6B). $Aicda^{cre/+}.Tsc1^{fl/fl}$ GC B cells were also enriched in cells with DZ phenotype, confirming a cell-intrinsic role for mTORC1 in regulating the LZ to DZ transition (Figures 6C and 6D). In spite of this enrichment, the proportion of $Aicda^{cre/+}.Tsc1^{fl/fl}$ B1-8^{hi} GC B cells decreased progressively over time (Figure 6E), indicating that unrestrained mTORC1 activity leads to a competitive disadvantage in GC selection. To ensure that lack of competitiveness was not a result of the

supra-physiological activation of mTOR driven by deletion of *Tsc1*, we performed a similar set of experiments using mice engineered to express a constitutively active allele of the RagA (*Rraga*) GTPase, *Rraga*[Q66L] (referred to hereafter as *Rraga*[GTP]) (Efeyan et al., 2013). Presence of this allele leads to loss of amino acid regulation of mTORC1, and only mild over-activation of this pathway. We bred the *Rraga*[GTP] allele to the B1-8[i] *Igh* (Sonoda et al., 1997), which also confers binding to NP when paired to an Igλ light chain, but with lower affinity than the B1-8[hi] allele [due to absence of an affinity-enhancing W to L mutation in position 33 (W33L) (Allen et al., 1988)]. Because *Rraga*[GTP/GTP] mice die perinatally (Efeyan et al., 2013), we generated fetal liver chimeras, and used these as B cell donors for adoptive transfer at 1:1 ratio with B1-8[i] cells with normal mTORC1 activity (Figure 6F). As with TSC1 deficiency, *Rraga*[GTP/GTP] GC B cells showed higher than normal mTOR activity (Figure 6G) and were moderately enriched in DZ phenotype (Figures 6H and 6I). Again, *Rraga*[GTP/GTP] B cells were strongly outcompeted in GCs over time (Figure 6J). Thus, although mTORC1 activation is essential for positive selection of GC B cells (Figure 4) and can favor the acquisition of a DZ phenotype normally associated with proliferation in a cell-autonomous manner, constitutive activation of this pathway does not on its own increase GC B cell competitiveness and is instead detrimental for GC selection.

To investigate whether constitutively active mTORC1 affects the ability of B cells to undergo affinity maturation, we immunized mTORC1 gain-of-function mice with NP-OVA in alum and measured the increase in titers of circulating total (NP$_{24}$-binding) and high-affinity (NP$_2$-binding) antibodies over a 28-day period by ELISA. To avoid any potential effects related to preferential selection of GC B cells that failed to recombine the floxed allele in *Aicda*[cre/+].*Tsc1*^{fl/fl} mice, we generated *Cd79a*[cre/+].*Tsc1*^{fl/fl} mice, in which recombination is triggered in a large fraction of B cells during development (Hobeika et al., 2006), making presence of unrecombined B cells in GCs less likely. Although *Cd79a*[cre/+].*Tsc1*^{fl/fl} mice produced NP-specific antibodies that were comparable in titer to those of *Cd79a*[cre/+].*Tsc1*^{+/+} littermates (Figure 7A), affinity maturation was almost entirely abrogated in these mice (Figure 7B). Analogous experiments using the *Rraga*[GTP] allele produced comparable results. Whereas global anti-NP titers upon immunization of hematopoietic chimeras made from *Rraga*[GTP/GTP] or *Rraga*^{+/+} fetal livers were similar (Figure 7C), *Rraga*[GTP/GTP] chimeras again were deficient in affinity maturation (Figure 7D), albeit to a lesser extent than *Cd79a*[cre/+].*Tsc1*^{fl/fl} mice. Because mTORC1 hyperactivation in chimeric mice is not B cell-specific, we performed additional experiments using adoptive transfer of B1-8[i] *Rraga*[GTP/GTP] or B1-8[i] *Rraga*^{+/+} B cells from fetal liver chimeras into WT mice, which we then immunized subcutaneously with NP-OVA in alum. *Igh* sequencing of single-sorted GC B cells from draining lymph nodes of recipient mice at day 12 after immunization showed that, although somatic mutations accumulated to a similar extent in both cases (Figure 7E), *Rraga*[GTP/GTP] GC B cells that acquired the affinity-enhancing W33L mutation were enriched to a significantly lower extent than their *Rraga*^{+/+} counterparts (Figure 7F). We conclude that uncoupling mTORC1 activity from affinity-dependent selection impairs the accumulation of high-affinity B cells in GCs, as well as in the antibody secreting cell compartment.

DISCUSSION

B cells selected in the GC LZ activate pathways that act in concert to enable their rapid clonal expansion in the DZ. We now show that, in addition to activating c-Myc and other transcriptional regulators, T cell help also drives activation of the mTORC1 pathway in GC B cells, promoting a phase of anabolic growth that precedes and sustains the successive cycles of DZ proliferation. mTORC1 activity in positively selected GC B cells can be modulated by varying either the dose of DEC-OVA or the ratio of *Ly75*^{+/+} to *Ly75*^{−/−} B cells, which alters the degree of competition for Tfh cells among this population. Because extent of T cell help also defines the magnitude of the ensuing proliferative burst (Gitlin et al., 2014), our findings point to a quantitative link between T cell help, mTORC1 activation and the number of division cycles a GC B cell can withstand following LZ to DZ transition.

Injection of the mTORC1 inhibitor rapamycin prior to cell growth markedly impaired the extent to which B cells accumulate upon forced positive selection. This effect occurred without measurable impact on cell cycle progression, regardless of the timing of rapamycin administration. These results indicate that the primary role of mTORC1 in GC selection is to ensure that B cells have sufficient biomass and growth potential to support rapid and repeated division cycles, rather than to directly control cell cycling. These data are in contrast to the notion that mTORC1 directly drives cell-cycle progression (Aagaard-Tillery and Jelinek, 1994; Fingar et al., 2004) but are consistent with an anabolic role for mTORC1 in cell division (Barbet et al., 1996; Dowling et al., 2010). Thus, while anabolism and proliferation are necessarily co-regulated and tend to occur simultaneously, in the process of GC B cell selection these two are spatially and temporally segregated, and depend on mTORC1 to different extents.

mTORC1 also has a marked effect on the DZ to LZ ratio of GC B cells that appears to be stronger than, and independent of, its effects on population expansion. Rapamycin treatment reproducibly decreased the proportion of B cells in the DZ even in conditions where expansion is unaffected, and conversely, mTORC1 hyperactivation led to accumulation of B cells in the DZ without increasing proliferation. This finding might be explained by an indirect effect of mTORC1 on the activity of Foxo1, a key regulator of the DZ phenotype (Dominguez-Sola et al., 2015; Sander et al., 2015). In agreement, our data show that rapamycin treatment prevents upregulation of Foxo1 upon induction of positive selection by DEC-OVA. We speculate that failure to upregulate Foxo1 might prevent establishment of the DZ program without affecting the cell cycle. Such uncoupling is similar to that observed upon specific deletion of Foxo1 in GC B cells (Dominguez-Sola et al., 2015; Sander et al., 2015).

The full extent to which c-Myc and mTORC1 synergize and cross-regulate during anabolic responses remains to be determined. Our experiments show that rapamycin treatment leads only to mild downregulation of c-Myc signature genes and c-Myc protein in selected B cells. This is in agreement with prior observations showing that optimal translation of c-Myc mRNA in lymphocytes requires mTORC1 (Verbist et al., 2016; West et al., 1998; Yang et al., 2013b). However, although rapamycin-sensitive mTORC1 signals are necessary for cell growth and clonal
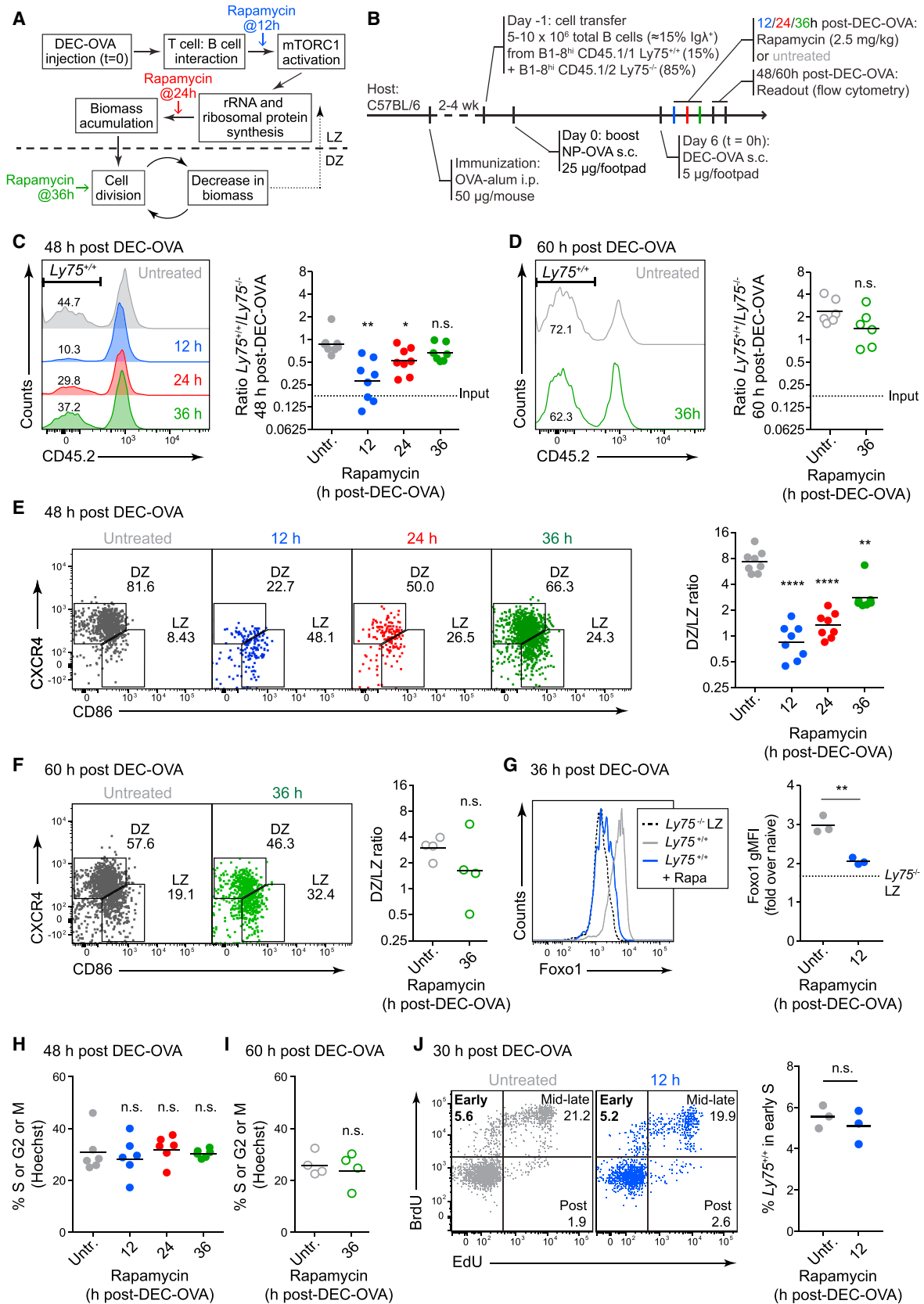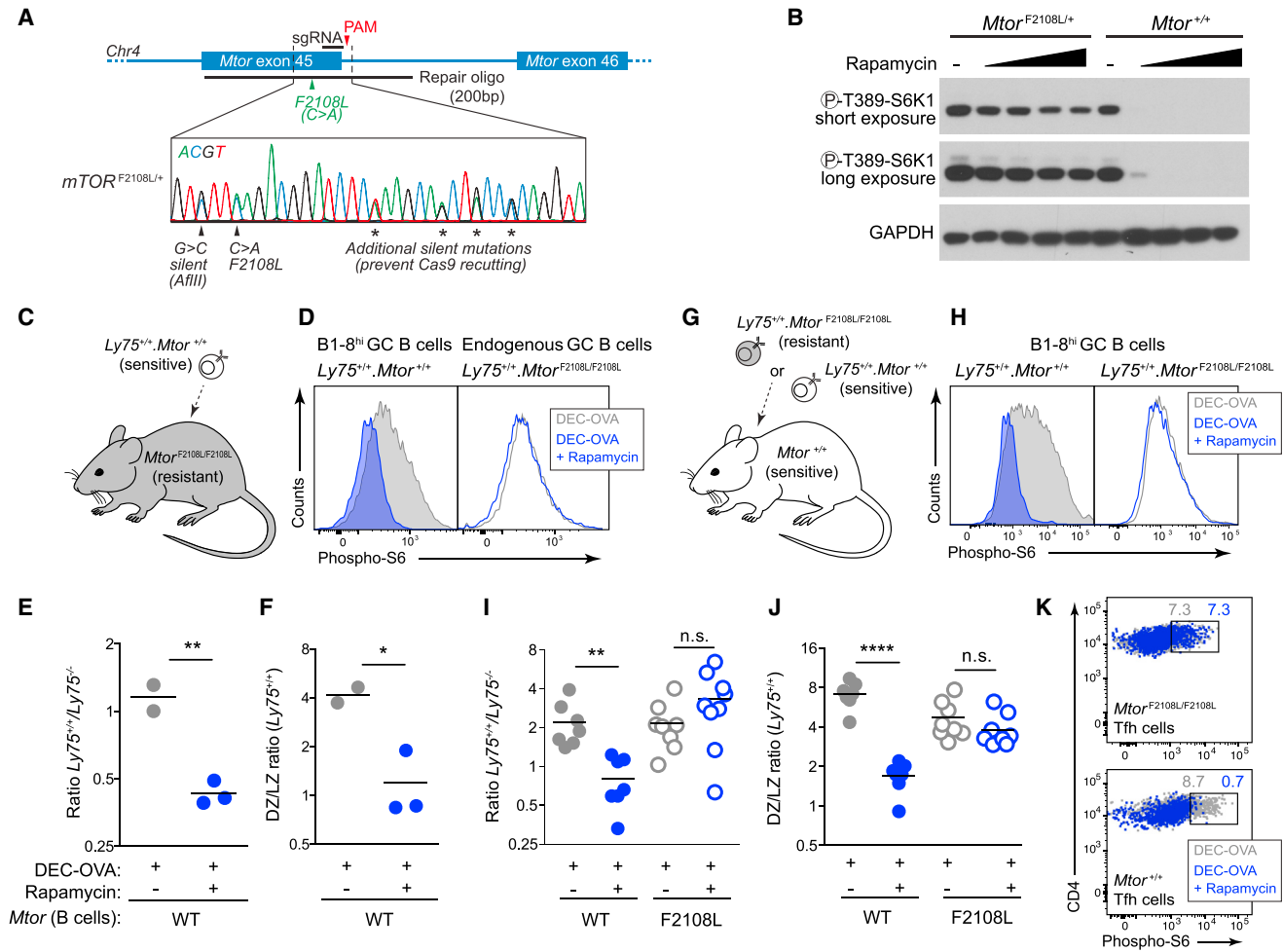
(legend on next page)

Figure 5. B Cell-Intrinsic Role of mTORC1 in GC Selection

(A) CRISPR/Cas9 gene targeting strategy for generating mice carrying F2108L mutation in *Mtor*.

(B) Immunoblots from tail fibroblasts from $Mtor^{+/+}$ and $Mtor^{F2108L/+}$ animals cultured in presence and absence of rapamycin.

(C) Rapamycin-resistant hosts received adoptive transfer of B1-8[hi] $L75^{+/+}.Mtor^{+/+}$ B cells for targeted selection in GCs by DEC-OVA injection 12 hr prior to rapamycin treatment (see Figure S5A).

(D) Phospho-S6 staining in transferred $L75^{+/+}.Mtor^{+/+}$ and host $Ly75^{+/+}.Mtor^{F2108L/F2108L}$ GC B cells.

(E) $Ly75^{+/+}/Ly75^{-/-}$ ratio and (F) DZ/LZ ratio in $Ly75^{+/+}.Mtor^{+/+}$ GC B cells.

(G) Wild-type hosts received adoptive transfer of B1-8[hi] $Ly75^{+/+}.Mtor^{+/+}$ or B1-8[hi] $L75^{+/+}.Mtor^{F2108L/F2108L}$ B cells for targeted selection in GCs by DEC-OVA injection 12 hr prior to rapamycin treatment (see Figure S5E).

(H) Phospho-S6 staining of transferred $Ly75^{+/+}.Mtor^{+/+}$ or $Ly75^{+/+}.Mtor^{F2108L/F2108L}$ cells treated or not with rapamycin.

(I) $Ly75^{+/+}/Ly75^{-/-}$ ratio and (J) DZ/LZ ratio of transferred $Ly75^{+/+}$ cells in GCs.

(K) Phospho-S6 staining in Tfh cells (CXCR5^{+} PD-1^{hi}) from $Mtor^{F2108L/F2108L}$ (see C) and $Mtor^{+/+}$ (see G) mice treated or not with rapamycin. Note that Tfh cells from $Mtor^{F2108L/F2108L}$ mice are fully resistant to rapamycin. *p < 0.05, **p < 0.01, ****p < 0.0001, n.s., non-significant unpaired Student's t test. Bars indicate mean. Data pooled from at least two independent experiments. (C–F, n = 2–3; G–J, n = 7–9; K n = 2–9) See also Figures S4 and S5.

expansion, they appear to be dispensable for cell cycle progression in our model. Given the strong association between c-Myc and cell cycle (Amati et al., 1998; Dominguez-Sola et al., 2007; Obaya et al., 1999), this suggests that the effects of rapamycin on clonal expansion are unlikely to be mediated solely by decreased c-Myc activity.

Figure 4. mTORC1-Induced Cell Growth Is Required for Expansion and Accumulation in DZ of Positively Selected B Cells

(A and B) Experimental setup for DEC-OVA-induced positive selection of $Ly75^{+/+}$ GC B cells followed by mTORC1 inhibition using rapamycin before, midway through, or after cell growth and LZ to DZ migration.

(C–J) Clonal expansion (C and D), DZ accumulation (E and F), Foxo1 upregulation (G), DNA content (Hoechst) (H and I), and S phase entry (J) among $Ly75^{+/+}$ GC B cells upon treatment with rapamycin at the indicated time points after DEC-OVA injection. S phase entry (J) is measured by sequential injection of EdU followed by BrdU 1 hr later. Cells in early S phase are positive for BrdU only (see STAR Methods). *p < 0.05, **p < 0.01, ****p < 0.0001, n.s. non-significant, unpaired Student t test, compared to rapamycin-untreated group. Bars indicate mean. Data pooled from at least two independent experiments. (C, n = 8; D, n = 6; E, n = 8; F, n = 4; G, n = 3; H, n = 6; I, n = 4; J, n = 3). See also Figure S3.
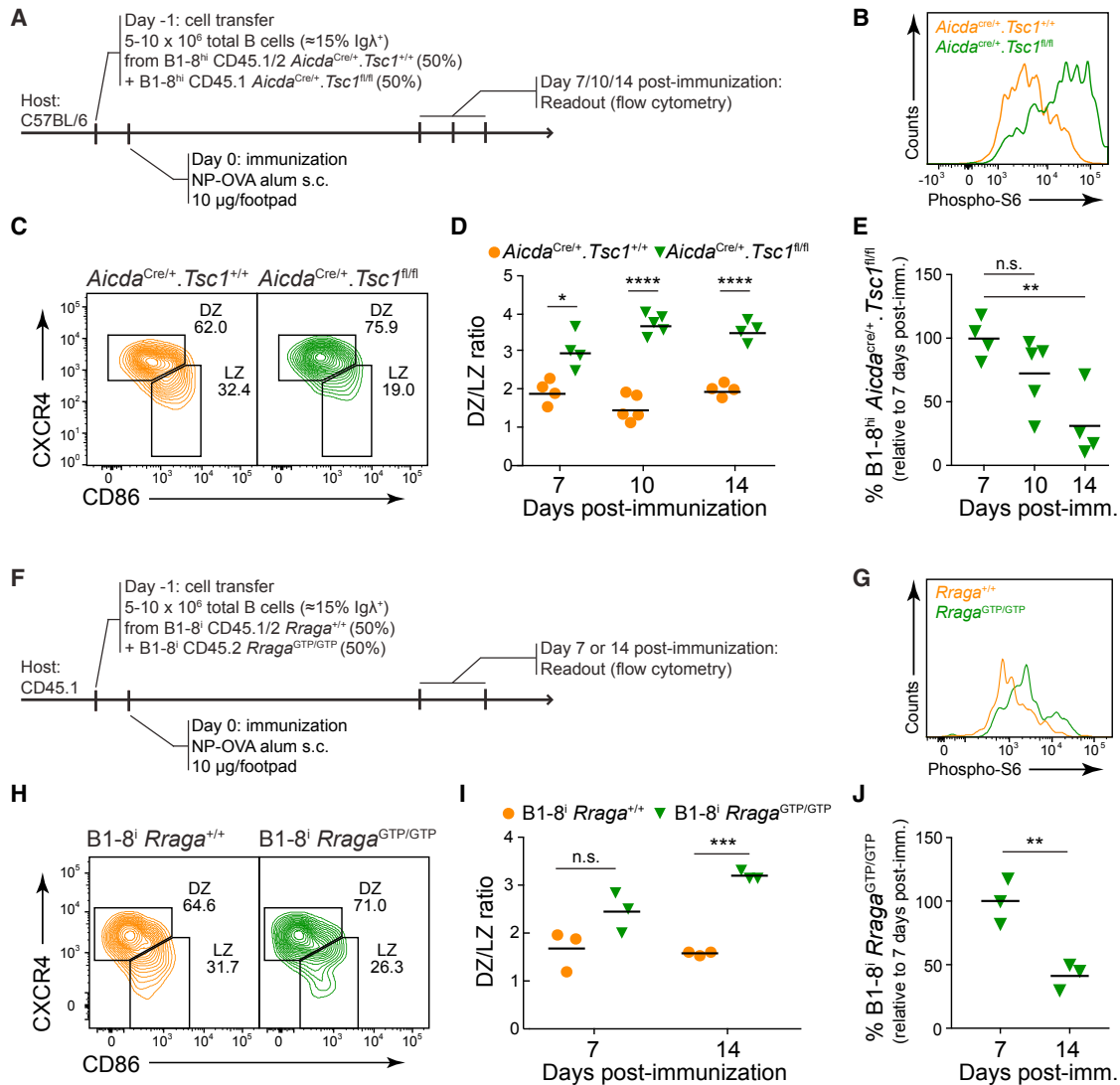
Figure 6. Hyperactivation of mTORC1 Imposes DZ Confinement and a Competitive Disadvantage on GC B Cells

(A) Experimental setup for induction of GCs containing mixtures of B1-8^hi cells sufficient and deficient in *Tsc1* upon AID-mediated deletion.

(B) Phospho-S6 in GC B1-8^hi cells 10 days after NP-OVA immunization.

(C) DZ and LZ staining in GC B1-8^hi cells 10 days after NP-OVA immunization, quantified over time in (D).

(E) Relative percentage (normalized to day 7 after immunization) of *Tsc1*-deficient GC B cells at the indicated time points after NP-OVA injection.

(F) Experimental setup for induction of GCs containing mixtures of B1-8^i cells carrying *Rraga*^+/+ and *Rraga*^GTP/GTP.

(G–J) As in (B–E) but using *Rraga*^GTP/GTP as an mTORC1 gain-of-function allele. (G)-(H) are from 7 days post-immunization. B cell donors were either full-body mutant mice or bone marrow chimeras (see STAR Methods). *p < 0.05, **p < 0.01, ***p < 0.001, ****p < 0.0001, n.s. non-significant unpaired Student t test. Bars indicate mean. Data pooled from at least two independent experiments (A–E, n = 4–5; F–J, n = 3).

B cells with constitutively high mTORC1 activity due to genetic loss of TSC1 or constitutive RagA activation were outcompeted by cells with wild-type mTORC1 activity. This is in spite of the fact that B cells lacking *Tsc1* are fully competent to form GCs when in the absence of competition with WT cells (Ci et al., 2015), ruling out deleterious effects of mTORC1 hyperactivation on GC B cell viability. A potential explanation for this disadvantage is that the failure of B cells to downregulate mTORC1 in the DZ might lead to excessive retention in this compartment and consequently decreased access to antigen and Tfh cells in the LZ. This would explain the decreased GC B cell competitiveness, as well as the impaired affinity maturation in mTOR gain-of-function models, given the tight dependence of affinity maturation on the spacing of proliferation and selection cycles (Kepler and Perelson, 1993). More broadly, our data are in line with previous reports showing that both mice and humans with constitutive hyperactivity of the upstream PI3K/Akt pathway show impaired humoral responses (Lucas et al., 2014; Suzuki et al., 2003), although the relative contribution of mTORC1 versus other targets of PI3K/Akt (e.g., Foxo1) to these phenotypes is unclear.

We therefore propose a model in which dynamic regulation of mTORC1 activity during the cyclic re-entry process supports
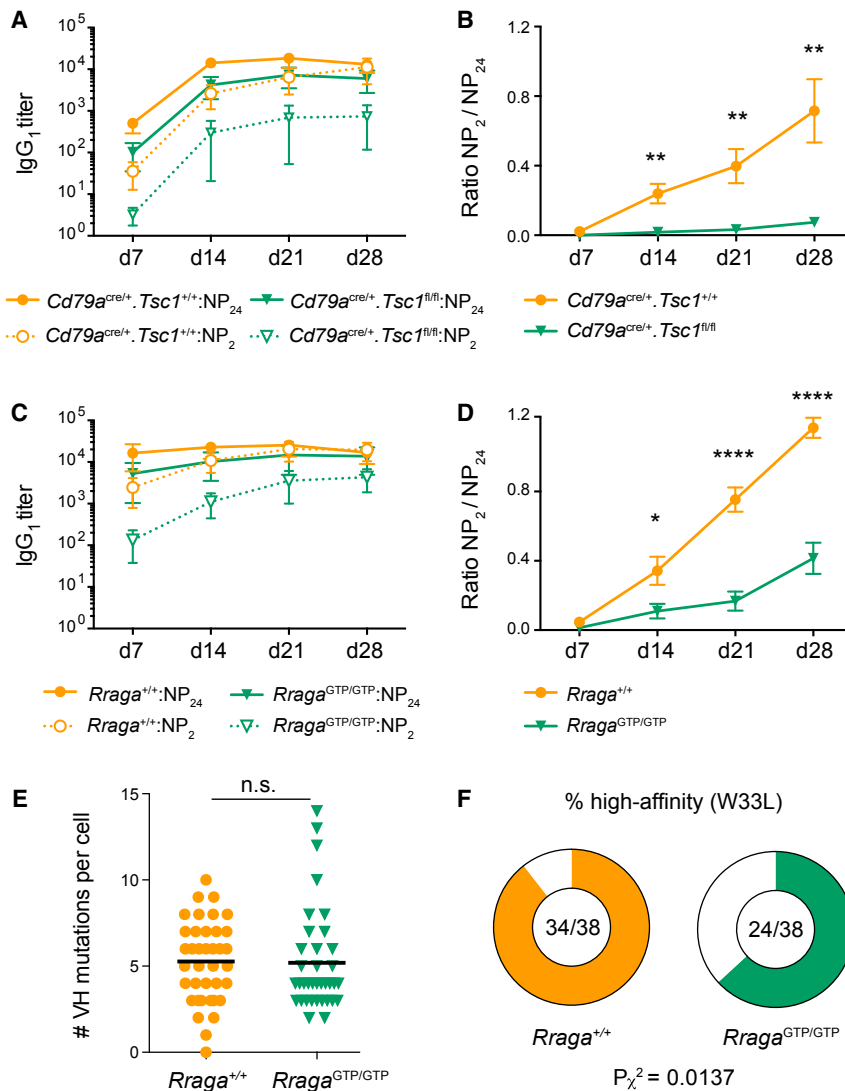
Figure 7. mTORC1 Hyperactivation Impairs Affinity Maturation

$Cd79a^{cre/+}.Tsc1^{+/+}$ and $Cd79a^{cre/+}.Tsc1^{fl/fl}$ bone marrow chimeras (see STAR Methods) were immunized i.p. with 50 μg of NP-OVA and serum was obtained at the indicated time points post-immunization.

(A) Titers of total (NP_{24}-binding) and high-affinity (NP_2-binding) antibodies and (B) NP_2/NP_{24} titer ratio in these mice.

(C and D) as in (A) and (B) but using $Rraga^{+/+}$ and $Rraga^{GTP/GTP}$ fetal liver chimeras.

(E) Total number of V_H mutations and (F) number of W33L high-affinity mutations in single-cell sorted GC B cells from wild-type mice adoptively transferred with B1-8^i $Rraga^{+/+}$ or B1-8^i $Rraga^{GTP/GTP}$ B cells, obtained from popliteal lymph nodes harvested 12 days after immunization with NP-OVA. Data pooled from two independent experiments. *$p < 0.05$, **$p < 0.01$, ****$p < 0.0001$, n.s. non-significant, unpaired Student's t test. In (A)–(D), bars indicate mean ± SEM; in (E) bars indicate mean (A and B, n = 8–9; C and D, n = 8; E and F, n = 2).

positive selection in the GC. In the LZ, mTORC1 is induced in positively selected B cells, promoting an increase in anabolic capacity (manifested as an increase in biomass and ribosome content) that supports subsequent proliferation and clonal expansion. Although the rapamycin-sensitive arm of mTORC1 does not directly control cell-cycle progression in these cells, decreases in mTORC1 activity and cell size are closely related with cessation of proliferation, likely due to the coordinated induction of a proliferative program through c-Myc or other pathways. Our data are also consistent with the need for decay in mTORC1 activity as cells proliferate in the DZ. Such decay appears to be required for a timely return of B cells from DZ to LZ, and GCs that fail to modulate mTORC1 activity are unable to discern cells that have acquired mutations that improve affinity, thus disabling affinity maturation.

Finally, to overcome the caveats related to the lack of cellular specificity of a chemical inhibitor such as rapamycin, we generated a strain of mice harboring a tumor-derived mutation in *Mtor* that renders the kinase insensitive to the drug. Rescue of the rapamycin phenotype when only transferred B cells carried the $Mtor^{F2108L}$ mutation confirmed that mTORC1 was required in a B cell-specific manner, rather than acting through other relevant cell types that rely on this pathway for differentiation and function, such as Tfh cells (Ray et al., 2015; Yang et al., 2016; Zeng et al., 2016). We expect that this chemical-genetics approach, and the $Mtor^{F2108L}$ mice in particular, will be useful to others to address the roles of mTORC1 in other settings, without the kinetic limitations of conditional mouse genetics.

STAR★METHODS

Detailed methods are provided in the online version of this paper and include the following:

- KEY RESOURCES TABLE
- CONTACT FOR REAGENT AND RESOURCE SHARING
- EXPERIMENTAL MODEL AND SUBJECT DETAILS
  - Mice

SUPPLEMENTAL INFORMATION

Supplemental Information includes five figures and can be found with this article online at http://dx.doi.org/10.1016/j.immuni.2017.06.005.

REFERENCES

Aagaard-Tillery, K.M., and Jelinek, D.F. (1994). Inhibition of human B lymphocyte cell cycle progression and differentiation by rapamycin. Cell. Immunol. *156*, 493–507.

Allen, D., Simon, T., Sablitzky, F., Rajewsky, K., and Cumano, A. (1988). Antibody engineering for the analysis of affinity maturation of an anti-hapten response. EMBO J. *7*, 1995–2001.

Allen, C.D., Okada, T., and Cyster, J.G. (2007). Germinal-center organization and cellular dynamics. Immunity *27*, 190–202.

Amati, B., Alevizopoulos, K., and Vlach, J. (1998). Myc and the cell cycle. Frontiers in bioscience: a journal and virtual library *3*, d250-268.

Araki, K., Turner, A.P., Shaffer, V.O., Gangappa, S., Keller, S.A., Bachmann, M.F., Larsen, C.P., and Ahmed, R. (2009). mTOR regulates memory CD8 T-cell differentiation. Nature *460*, 108–112.

Bannard, O., Horton, R.M., Allen, C.D., An, J., Nagasawa, T., and Cyster, J.G. (2013). Germinal center centroblasts transition to a centrocyte phenotype according to a timed program and depend on the dark zone for effective selection. Immunity *39*, 912–924.

Bannard, O., McGowan, S.J., Ersching, J., Ishido, S., Victora, G.D., Shin, J.S., and Cyster, J.G. (2016). Ubiquitin-mediated fluctuations in MHC class II facilitate efficient germinal center B cell responses. J. Exp. Med. *213*, 993–1009.

Barbet, N.C., Schneider, U., Helliwell, S.B., Stansfield, I., Tuite, M.F., and Hall, M.N. (1996). TOR controls translation initiation and early G1 progression in yeast. Mol. Biol. Cell *7*, 25–42.

Boscardin, S.B., Hafalla, J.C., Masilamani, R.F., Kamphorst, A.O., Zebroski, H.A., Rai, U., Morrot, A., Zavala, F., Steinman, R.M., Nussenzweig, R.S., and Nussenzweig, M.C. (2006). Antigen targeting to dendritic cells elicits long-lived T cell help for antibody responses. J. Exp. Med. *203*, 599–606.

Calado, D.P., Sasaki, Y., Godinho, S.A., Pellerin, A., Köchert, K., Sleckman, B.P., de Alborán, I.M., Janz, M., Rodig, S., and Rajewsky, K. (2012). The cell-cycle regulator c-Myc is essential for the formation and maintenance of germinal centers. Nat. Immunol. *13*, 1092–1100.

Chou, C., Verbaro, D.J., Tonc, E., Holmgren, M., Cella, M., Colonna, M., Bhattacharya, D., and Egawa, T. (2016). The Transcription Factor AP4 Mediates Resolution of Chronic Viral Infection through Amplification of Germinal Center B Cell Responses. Immunity *45*, 570–582.

Ci, X., Kuraoka, M., Wang, H., Carico, Z., Hopper, K., Shin, J., Deng, X., Qiu, Y., Unniraman, S., Kelsoe, G., and Zhong, X.P. (2015). TSC1 Promotes B Cell Maturation but Is Dispensable for Germinal Center Formation. PLoS ONE *10*, e0127527.

Dominguez-Sola, D., Ying, C.Y., Grandori, C., Ruggiero, L., Chen, B., Li, M., Galloway, D.A., Gu, W., Gautier, J., and Dalla-Favera, R. (2007). Non-transcriptional control of DNA replication by c-Myc. Nature *448*, 445–451.

Dominguez-Sola, D., Victora, G.D., Ying, C.Y., Phan, R.T., Saito, M., Nussenzweig, M.C., and Dalla-Favera, R. (2012). The proto-oncogene MYC is required for selection in the germinal center and cyclic reentry. Nat. Immunol. *13*, 1083–1091.

Dominguez-Sola, D., Kung, J., Holmes, A.B., Wells, V.A., Mo, T., Basso, K., and Dalla-Favera, R. (2015). The FOXO1 Transcription Factor Instructs the Germinal Center Dark Zone Program. Immunity *43*, 1064–1074.

Dowling, R.J., Topisirovic, I., Alain, T., Bidinosti, M., Fonseca, B.D., Petroulakis, E., Wang, X., Larsson, O., Selvaraj, A., Liu, Y., et al. (2010). mTORC1-mediated cell proliferation, but not cell growth, controlled by the 4E-BPs. Science *328*, 1172–1176.

Efeyan, A., Zoncu, R., Chang, S., Gumper, I., Snitkin, H., Wolfson, R.L., Kirak, O., Sabatini, D.D., and Sabatini, D.M. (2013). Regulation of mTORC1 by the Rag GTPases is necessary for neonatal autophagy and survival. Nature *493*, 679–683.

Efeyan, A., Schweitzer, L.D., Bilate, A.M., Chang, S., Kirak, O., Lamming, D.W., and Sabatini, D.M. (2014). RagA, but not RagB, is essential for embryonic development and adult mice. Dev. Cell *29*, 321–329.

Eisen, H.N., and Siskind, G.W. (1964). Variations in Affinities of Antibodies during the Immune Response. Biochemistry *3*, 996–1008.

Fingar, D.C., Richardson, C.J., Tee, A.R., Cheatham, L., Tsou, C., and Blenis, J. (2004). mTOR controls cell cycle progression through its cell growth effectors S6K1 and 4E-BP1/eukaryotic translation initiation factor 4E. Mol. Cell. Biol. *24*, 200–216.

Gitlin, A.D., Shulman, Z., and Nussenzweig, M.C. (2014). Clonal selection in the germinal centre by regulated proliferation and hypermutation. Nature *509*, 637–640.

Gitlin, A.D., Mayer, C.T., Oliveira, T.Y., Shulman, Z., Jones, M.J., Koren, A., and Nussenzweig, M.C. (2015). HUMORAL IMMUNITY. T cell help controls the speed of the cell cycle in germinal center B cells. Science *349*, 643–646.

Hobeika, E., Thiemann, S., Storch, B., Jumaa, H., Nielsen, P.J., Pelanda, R., and Reth, M. (2006). Testing gene function early in the B cell lineage in mb1-cre mice. Proc. Natl. Acad. Sci. USA 103, 13789–13794.

Huang, C.Y., Bredemeyer, A.L., Walker, L.M., Bassing, C.H., and Sleckman, B.P. (2008). Dynamic regulation of c-Myc proto-oncogene expression during lymphocyte development revealed by a GFP-c-Myc knock-in mouse. Eur. J. Immunol. 38, 342–349.

Inaba, K., Swiggard, W.J., Inaba, M., Meltzer, J., Mirza, A., Sasagawa, T., Nussenzweig, M.C., and Steinman, R.M. (1995). Tissue distribution of the DEC-205 protein that is detected by the monoclonal antibody NLDC-145. I. Expression on dendritic cells and other subsets of mouse leukocytes. Cell. Immunol. 163, 148–156.

Jones, D.D., Gaudette, B.T., Wilmore, J.R., Chernova, I., Bortnick, A., Weiss, B.M., and Allman, D. (2016). mTOR has distinct functions in generating versus sustaining humoral immunity. J. Clin. Invest. 126, 4250–4261.

Kamphorst, A.O., Guermonprez, P., Dudziak, D., and Nussenzweig, M.C. (2010). Route of antigen uptake differentially impacts presentation by dendritic cells and activated monocytes. J. Immunol. 185, 3426–3435.

Keating, R., Hertz, T., Wehenkel, M., Harris, T.L., Edwards, B.A., McClaren, J.L., Brown, S.A., Surman, S., Wilson, Z.S., Bradley, P., et al. (2013). The kinase mTOR modulates the antibody response to provide cross-protective immunity to lethal infection with influenza virus. Nat. Immunol. 14, 1266–1276.

Kepler, T.B., and Perelson, A.S. (1993). Cyclic re-entry of germinal center B cells and the efficiency of affinity maturation. Immunol. Today 14, 412–415.

Kwiatkowski, D.J., Zhang, H., Bandura, J.L., Heiberger, K.M., Glogauer, M., el-Hashemite, N., and Onda, H. (2002). A mouse model of TSC1 reveals sex-dependent lethality from liver hemangiomas, and up-regulation of p70S6 kinase activity in Tsc1 null cells. Hum. Mol. Genet. 11, 525–534.

Laplante, M., and Sabatini, D.M. (2012). mTOR signaling in growth control and disease. Cell 149, 274–293.

Limon, J.J., So, L., Jellbauer, S., Chiu, H., Corado, J., Sykes, S.M., Raffatellu, M., and Fruman, D.A. (2014). mTOR kinase inhibitors promote antibody class switching via mTORC2 inhibition. Proc. Natl. Acad. Sci. USA 111, E5076–E5085.

Lin, W.H., Adams, W.C., Nish, S.A., Chen, Y.H., Yen, B., Rothman, N.J., Kratchmarov, R., Okada, T., Klein, U., and Reiner, S.L. (2015). Asymmetric PI3K Signaling Driving Developmental and Regenerative Cell Fate Bifurcation. Cell Rep. 13, 2203–2218.

Lucas, C.L., Zhang, Y., Venida, A., Wang, Y., Hughes, J., McElwee, J., Butrick, M., Matthews, H., Price, S., Biancalana, M., et al. (2014). Heterozygous splice mutation in PIK3R1 causes human immunodeficiency with lymphoproliferation due to dominant activation of PI3K. J. Exp. Med. 211, 2537–2547.

MacLennan, I.C. (1994). Germinal centers. Annu. Rev. Immunol. 12, 117–139.

Mesin, L., Ersching, J., and Victora, G.D. (2016). Germinal Center B Cell Dynamics. Immunity 45, 471–482.

Obaya, A.J., Mateyak, M.K., and Sedivy, J.M. (1999). Mysterious liaisons: the relationship between c-Myc and the cell cycle. Oncogene 18, 2934–2941.

Omori, S.A., Cato, M.H., Anzelon-Mills, A., Puri, K.D., Shapiro-Shelef, M., Calame, K., and Rickert, R.C. (2006). Regulation of class-switch recombination and plasma cell differentiation by phosphatidylinositol 3-kinase signaling. Immunity 25, 545–557.

Pasqual, G., Angelini, A., and Victora, G.D. (2015). Triggering positive selection of germinal center B cells by antigen targeting to DEC-205. Methods Mol. Biol. 1291, 125–134.

Peng, T., Golub, T.R., and Sabatini, D.M. (2002). The immunosuppressant rapamycin mimics a starvation-like signal distinct from amino acid and glucose deprivation. Mol. Cell. Biol. 22, 5575–5584.

Powell, J.D., Pollizzi, K.N., Heikamp, E.B., and Horton, M.R. (2012). Regulation of immune responses by mTOR. Annu. Rev. Immunol. 30, 39–68.

Ray, J.P., Staron, M.M., Shyer, J.A., Ho, P.C., Marshall, H.D., Gray, S.M., Laidlaw, B.J., Araki, K., Ahmed, R., Kaech, S.M., and Craft, J. (2015). The Interleukin-2-mTORc1 Kinase Axis Defines the Signaling, Differentiation, and Metabolism of T Helper 1 and Follicular B Helper T Cells. Immunity 43, 690–702.

Robbiani, D.F., Bunting, S., Feldhahn, N., Bothmer, A., Camps, J., Deroubaix, S., McBride, K.M., Klein, I.A., Stone, G., Eisenreich, T.R., et al. (2009). AID produces DNA double-strand breaks in non-Ig genes and mature B cell lymphomas with reciprocal chromosome translocations. Mol. Cell 36, 631–641.

Sander, S., Calado, D.P., Srinivasan, L., Köchert, K., Zhang, B., Rosolowski, M., Rodig, S.J., Holzmann, K., Stilgenbauer, S., Siebert, R., et al. (2012). Synergy between PI3K signaling and MYC in Burkitt lymphomagenesis. Cancer Cell 22, 167–179.

Sander, S., Chu, V.T., Yasuda, T., Franklin, A., Graf, R., Calado, D.P., Li, S., Imami, K., Selbach, M., Di Virgilio, M., et al. (2015). PI3 Kinase and FOXO1 Transcription Factor Activity Differentially Control B Cells in the Germinal Center Light and Dark Zones. Immunity 43, 1075–1086.

Schaefer, B.C., Schaefer, M.L., Kappler, J.W., Marrack, P., and Kedl, R.M. (2001). Observation of antigen-dependent CD8+ T-cell/ dendritic cell interactions in vivo. Cell. Immunol. 214, 110–122.

Schuhmacher, M., Kohlhuber, F., Hölzel, M., Kaiser, C., Burtscher, H., Jarsch, M., Bornkamm, G.W., Laux, G., Polack, A., Weidle, U.H., and Eick, D. (2001). The transcriptional program of a human B cell line in response to Myc. Nucleic Acids Res. 29, 397–406.

Shih, T.A., Meffre, E., Roederer, M., and Nussenzweig, M.C. (2002). Role of BCR affinity in T cell dependent antibody responses in vivo. Nat. Immunol. 3, 570–575.

Shulman, Z., Gitlin, A.D., Weinstein, J.S., Lainez, B., Esplugues, E., Flavell, R.A., Craft, J.E., and Nussenzweig, M.C. (2014). Dynamic signaling by T follicular helper cells during germinal center B cell selection. Science 345, 1058–1062.

Sinclair, L.V., Finlay, D., Feijoo, C., Cornish, G.H., Gray, A., Ager, A., Okkenhaug, K., Hagenbeek, T.J., Spits, H., and Cantrell, D.A. (2008). Phosphatidylinositol-3-OH kinase and nutrient-sensing mTOR pathways control T lymphocyte trafficking. Nat. Immunol. 9, 513–521.

Sonoda, E., Pewzner-Jung, Y., Schwers, S., Taki, S., Jung, S., Eilat, D., and Rajewsky, K. (1997). B cell development under the condition of allelic inclusion. Immunity 6, 225–233.

Subramanian, A., Tamayo, P., Mootha, V.K., Mukherjee, S., Ebert, B.L., Gillette, M.A., Paulovich, A., Pomeroy, S.L., Golub, T.R., Lander, E.S., and Mesirov, J.P. (2005). Gene set enrichment analysis: a knowledge-based approach for interpreting genome-wide expression profiles. Proc. Natl. Acad. Sci. USA 102, 15545–15550.

Sun, K., Atoyan, R., Borek, M.A., Dellarocca, S., Samson, M.E., Ma, A.W., Xu, G.X., Patterson, T., Tuck, D.P., Viner, J.L., et al. (2017). Dual HDAC and PI3K Inhibitor CUDC-907 Downregulates MYC and Suppresses Growth of MYC-dependent Cancers. Mol. Cancer Ther. 16, 285–299.

Suzuki, A., Kaisho, T., Ohishi, M., Tsukio-Yamaguchi, M., Tsubata, T., Koni, P.A., Sasaki, T., Mak, T.W., and Nakano, T. (2003). Critical roles of Pten in B cell homeostasis and immunoglobulin class switch recombination. J. Exp. Med. 197, 657–667.

Tas, J.M., Mesin, L., Pasqual, G., Targ, S., Jacobsen, J.T., Mano, Y.M., Chen, C.S., Weill, J.C., Reynaud, C.A., Browne, E.P., et al. (2016). Visualizing antibody affinity maturation in germinal centers. Science 351, 1048–1054.

Trombetta, J.J., Gennert, D., Lu, D., Satija, R., Shalek, A.K., and Regev, A. (2014). Preparation of Single-Cell RNA-Seq Libraries for Next Generation Sequencing. Curr Protoc Mol Biol 107, 1–17.

Verbist, K.C., Guy, C.S., Milasta, S., Liedmann, S., Kamiński, M.M., Wang, R., and Green, D.R. (2016). Metabolic maintenance of cell asymmetry following division in activated T lymphocytes. Nature 532, 389–393.

Victora, G.D., and Nussenzweig, M.C. (2012). Germinal centers. Annu. Rev. Immunol. 30, 429–457.

Victora, G.D., Schwickert, T.A., Fooksman, D.R., Kamphorst, A.O., Meyer-Hermann, M., Dustin, M.L., and Nussenzweig, M.C. (2010). Germinal center dynamics revealed by multiphoton microscopy with a photoactivatable fluorescent reporter. Cell 143, 592–605.

Wagle, N., Grabiner, B.C., Van Allen, E.M., Amin-Mansour, A., Taylor-Weiner, A., Rosenberg, M., Gray, N., Barletta, J.A., Guo, Y., Swanson, S.J., et al.

(2014). Response and acquired resistance to everolimus in anaplastic thyroid cancer. N. Engl. J. Med. *371*, 1426–1433.

Wang, H., Yang, H., Shivalila, C.S., Dawlaty, M.M., Cheng, A.W., Zhang, F., and Jaenisch, R. (2013). One-step generation of mice carrying mutations in multiple genes by CRISPR/Cas-mediated genome engineering. Cell *153*, 910–918.

West, M.J., Stoneley, M., and Willis, A.E. (1998). Translational induction of the c-myc oncogene via activation of the FRAP/TOR signalling pathway. Oncogene *17*, 769–780.

Yang, H., Wang, H., Shivalila, C.S., Cheng, A.W., Shi, L., and Jaenisch, R. (2013a). One-step generation of mice carrying reporter and conditional alleles by CRISPR/Cas-mediated genome engineering. Cell *154*, 1370–1379.

Yang, K., Shrestha, S., Zeng, H., Karmaus, P.W., Neale, G., Vogel, P., Guertin, D.A., Lamb, R.F., and Chi, H. (2013b). T cell exit from quiescence and differentiation into Th2 cells depend on Raptor-mTORC1-mediated metabolic reprogramming. Immunity *39*, 1043–1056.

Yang, J., Lin, X., Pan, Y., Wang, J., Chen, P., Huang, H., Xue, H.H., Gao, J., and Zhong, X.P. (2016). Critical roles of mTOR Complex 1 and 2 for T follicular helper cell differentiation and germinal center responses. eLife *5*, 5.

Zeller, K.I., Jegga, A.G., Aronow, B.J., O'Donnell, K.A., and Dang, C.V. (2003). An integrated database of genes responsive to the Myc oncogenic transcription factor: identification of direct genomic targets. Genome Biol. *4*, R69.

Zeng, H., Yang, K., Cloer, C., Neale, G., Vogel, P., and Chi, H. (2013). mTORC1 couples immune signals and metabolic programming to establish T(reg)-cell function. Nature *499*, 485–490.

Zeng, H., Cohen, S., Guy, C., Shrestha, S., Neale, G., Brown, S.A., Cloer, C., Kishton, R.J., Gao, X., Youngblood, B., et al. (2016). mTORC1 and mTORC2 Kinase Signaling and Glucose Metabolism Drive Follicular Helper T Cell Differentiation. Immunity *45*, 540–554.

Zhang, S., Pruitt, M., Tran, D., Du Bois, W., Zhang, K., Patel, R., Hoover, S., Simpson, R.M., Simmons, J., Gary, J., et al. (2013). B cell-specific deficiencies in mTOR limit humoral immune responses. J. Immunol. *191*, 1692–1703.

Zheng, Y., Collins, S.L., Lutz, M.A., Allen, A.N., Kole, T.P., Zarek, P.E., and Powell, J.D. (2007). A role for mammalian target of rapamycin in regulating T cell activation versus anergy. J. Immunol. *178*, 2163–2170.

STAR★METHODS

KEY RESOURCES TABLE

REAGENT or RESOURCE	SOURCE	IDENTIFIER
Antibodies		
Rat monoclonal anti-CD16/CD32 (clone 2.4G2)	BioXCell	Cat#CUS-HB-197
Rat monoclonal anti-B220 PECy7 (clone RA3-6B2)	BioLegend	Cat#103222
Mouse monoclonal anti-BrdU FITC (clone 3D4)	BD Biosciences	Cat#51-23614L
Rat monoclonal anti-CD19 BV785 (clone 6D5)	BioLegend	Cat#115543
Rat monoclonal anti-CD38 PerCP-Cy5.5 (clone 90/CD38)	BD Biosciences	Cat#562770
Rat monoclonal anti-CD4 FITC (clone GK1.5)	BD Biosciences	Cat#561828
Mouse monoclonal anti-CD45.1 BV711 (clone A20)	BioLegend	Cat#110739
Mouse monoclonal anti-CD45.2 AF700 (clone 104)	BioLegend	Cat#109822
Rat monoclonal anti-CD83 Biotin (clone Michel-19)	BioLegend	Cat#121504
Rat monoclonal anti-CD86 AF488 (cone GL-1)	BioLegend	Cat#105018
Armenian Hamster monoclonal anti-CD95 PECy7 (clone Jo2)	BD Biosciences	Cat#557653
Rat monoclonal anti-CXCR4 PE (clone 2B11)	eBioscience	Cat#12-9991-82
Rat monoclonal anti-CXCR5 BV421 (clone L138D7)	BioLegend	Cat#145511
Rabbit monoclonal anti-Foxo1 PE (clone C29H4)	CST	Cat#14262S
Rat monoclonal anti-PD-1 APCCy7 (clone 29F.1A12)	BioLegend	Cat#135224
Rabbit monoclonal anti-PhosphoS6 (Ser235/236) AF647 (clone D57.2.2E)	CST	Cat#4851S
Rat monoclonal anti-AID (clone mAID-2)	eBioscience	Cat#14-5959-82
Goat polyclonal anti-Rat AF555	Invitrogen	Cat#A-21434
Rabbit monoclonal anti-c-Myc (clone D84C12)	CST	Cat#5605S
Goat polyclonal anti-Rabbit AF488	Invitrogen	Cat#A31627
Rat monoclonal anti-CD35 (clone 8C12)	BD biosciences	Cat#558768
Armenian Hamster monoclonal anti-CD40L (clone MR-1)	BioXCell	Cat#BE0017-1
Armenian Hamster polyclonal IgG	BioXCell	Cat#BE0091
Rat monoclonal anti-CD40 (clone FGK4.5)	BioXCell	Cat#BE0016-2
Rat monoclonal IgG2a (clone 2A3)	BioXCell	Cat#BE0089
Rabbit monoclonal anti-Phospho-p70 S6K (Thr389) (clone108D2)	CST	Cat#9234
Rabbit polyclonal anti-Phospho-S6 (Ser240/244)	CST	Cat#2215
Rabbit monoclonal anti-Phospho-4E-BP1 (Thr37/46) (clone 236B4)	CST	Cat#2855
Rabbit monoclonal anti-Phospho-Akt (Thr308) (clone C31E5E)	CST	Cat#2965
Rabbit monoclonal anti-Phospho-Akt (Ser473) (clone D9E)	CST	Cat#4060
Rabbit monoclonal anti-Akt (pan) (clone C67E7)	CST	Cat#4691
Rabbit monoclonal anti-p70 S6K (clone 49D7)	CST	Cat#2708
Rabbit monoclonal anti-4E-BP1 (clone 53H11)	CST	Cat#9644
Rabbit monoclonal anti-S6 (clone 5G10)	CST	Cat#2217
Rabbit monoclonal anti-mTOR (clone 7C10)	CST	Cat#2983

(Continued on next page)

Continued

REAGENT or RESOURCE	SOURCE	IDENTIFIER
Goat polyclonal anti-IgG1 HRP	SouthernBiotech	Cat#1070-05
Recombinant Anti-DEC-205-OVA	Pasqual et al., 2015	N/A
Recombinant Anti-DEC-205-CS	Boscardin et al., 2006	N/A
Chemicals, Peptides, and Recombinant Proteins		
2-NBDG	Invitrogen	Cat#N13195
BrdU	Sigma	Cat#B5002-1G
Click-iT Plus AF647	Invitrogen	Cat#C10634
EdU	Carbosynth	Cat#NE08701
Hoechst 33342	Invitrogen	Cat#H3570
Pyronin Y	Sigma	Cat#P9172-1G
Streptavidin BV421	BioLegend	Cat#405226
Streptavidin APC	BioLegend	Cat#405207
Streptavidin APC-eFluor780	eBioscience	Cat#47-4317-82
NP$_{(16)}$-OVA	Bioserach Technologies	Cat#N-5051-100
Rapamycin	LC Laboratories	Cat#R-5000
KLH	Sigma	Cat#H8283
NP$_{(19)}$-KLH	Conjugated in house	N/A
NP$_{(2)}$-BSA	Conjugated in house	N/A
NP$_{(24)}$-BSA	Conjugated in house	N/A
NP-PE	Biosearch Technologies	Cat#N-5070-1
Critical Commercial Assays		
Agencourt RNAClean XP kit	Beckman Coulter	Cat#A63987
Texas Red-X	Life Technologies	Cat#T20175
CD43 MicroBeads	Miltenyi Biotec	Cat#130-049-801
TCL Buffer	Qiagen	Cat#1031576
Avidin/Biotin Blocking Kit	Vector Laboratories	Cat#SP-2001
MEGAshortscript T7 transcription kit	Life Technologies	Cat#AM1354
Deposited Data		
RNA sequencing data	This paper	GEO: GSE98778
Experimental Models: Organisms/Strains		
Mouse: C57BL6/J	The Jackson Laboratory	JAX: 000664
Mouse: B1-8^{i}	The Jackson Laboratory	JAX: 012642
Mouse: PA-GFP	The Jackson Laboratory	JAX: 022486
Mouse: ECFP	The Jackson Laboratory	JAX: 004218
Mouse: *Tsc1*$^{fl/fl}$	The Jackson Laboratory	JAX: 005680
Mouse: *Rraga*^{GTP}	Efeyan et al., 2013	N/A
Mouse: *Mtor*^{F2108L}	This paper	N/A
Mouse: *Aicda*^{Cre}	Robbiani et al., 2009	N/A
Mouse: B1-8^{hi}	Shih et al., 2002	N/A
Mouse: *LY75*-tg	Kamphorst et al., 2010	N/A
Mouse: *Myc*^{GFP}	Huang et al., 2008	N/A
Mouse: *Cd79a*^{Cre}	Hobeika et al., 2006	N/A
Oligonucleotides		
dsDNA template for chimeric sgRNA transcription (protospacer sequence in capital letters): cgctgttaatacgactcactataggGATCTCAAAGCAGCTACCCCgttttagagctagaaatagcaagttaaaataaggctagtccgttatcaacttgaaaaagtggcaccgagtcggtgctttt	This paper	N/A

Continued

REAGENT or RESOURCE	SOURCE	IDENTIFIER
Repair oligo (differences from original C57BL6 sequence are in uppercase; mutations upstream of the AflII site were for use with a different sgRNA, and were not incorporated into the resulting mouse strain): tatggccgagatttaatggaggcacaagaatggtgtc gaaagtacatgaagtcggggaacgtcaaAgaTctGacgca GgcctgggacctctactatcacgtCttAagacggatctcTaag caActGccGcaggtaggctctcgaggcatcctgggttcatc tgtgcatccagactcgcttctgctggagacttatagaaa	This paper	N/A
F2108L genotyping primer Forward GCCACCTTGGTAGCTTGAAA	This paper	N/A
F2108L genotyping primer Reverse GTTGGGGTCGTATGTTCCTG	This paper	N/A
Software and Algorithms		
Gene Pattern	Broad Institute	http://software.broadinstitute.org/cancer/software/genepattern/
Flowjo v.8.7 and v.10.0.8r1	Flowjo	https://www.flowjo.com/
Prism 7	GraphPad	http://www.graphpad.com/scientific-software/prism/
Kallisto v0.43.0	Bray et al., 2016	https://pachterlab.github.io/kallisto/about.html
GSEA software v2.2.3	Tamayo et al., 2003	http://software.broadinstitute.org/gsea/index.jsp
Illustrator CS5	Adobe Systems Inc.	N/A

CONTACT FOR REAGENT AND RESOURCE SHARING

Further information and requests for reagents and resources should be directed to and will be fulfilled by the Lead Contact Gabriel D. Victora (victora@rockefeller.edu). The mouse lines obtained from other laboratories are described bellow and may require a Material Transfer Agreement (MTA) with the providing scientists. DEC-OVA plasmids were obtained from M. Nussenzweig (Rockefeller University, New York, USA) and require an MTA. $Mtor^{F2108L}$ mice generated in this study are available from our laboratory, also with an MTA.

EXPERIMENTAL MODEL AND SUBJECT DETAILS

Mice

C57BL6/J, B1-8[i] (Sonoda et al., 1997), PA-GFP (Victora et al., 2010), ECFP-transgenic (Schaefer et al., 2001) and $Tsc1^{fl/fl}$ (Kwiatkowski et al., 2002) mice were purchased from Jackson Labs (Strain numbers 000664, 012642, 022486, 004218, and 005680 respectively). $Rraga^{GTP}$ (Efeyan et al., 2013) and $Mtor^{F2108L}$ mice were generated and maintained in our laboratories. $Aicda^{cre}$ (Robbiani et al., 2009), B1-8[hi] (Shih et al., 2002), $Ly75^{-/-}$ (Inaba et al., 1995), and $LY75$-tg (which express human DEC-205 under the CD11c promoter) (Kamphorst et al., 2010) mice were originally provided by M. Nussenzweig (Rockefeller University, New York, USA). Myc^{GFP} mice (Huang et al., 2008) were a generated originally by B. Sleckman (Weill Cornell Medicine, New York, USA) and were provided to us by R. Dalla-Favera (Columbia University, New York, USA). $Cd79a^{cre/+}$ mice (Hobeika et al., 2006) were provided by M. Reth (Max Planck Institute, Freiburg, Germany). Because we observed debilitating or lethal off-target effects of $Cd79a^{cre/+}$ mediated deletion of $Tsc1$ in the kidneys, affinity maturation ELISA experiments were preformed with bone marrow chimeras in which lethally irradiated wild-type hosts were reconstituted with $Cd79a^{cre/+}.Tsc1^{fl/fl}$ or $Cd79a^{cre/+}.Tsc1^{+/+}$ bone marrows. All mice were housed in groups of 2-5 animals per cage in specific pathogen-free facilities at the Whitehead Institute for Biomedical Research and The Rockefeller University. All protocols were approved by the Massachusetts Institute of Technology Committee for Animal Care and the Rockefeller University Institutional Animal Care and Use Committee. Males and females, 6-8 week-old mice were used in the experiments. When adoptive cell transfer was performed, host animals were invariably males.

METHOD DETAILS

Cell Transfers, Immunizations, and Treatments

Spleens were macerated, red blood cells were lysed with ACK buffer (Lonza), and resulting cell suspensions were filtered through a 70 μm mesh into PBS supplemented with 0.5% BSA and 2 mM EDTA (PBE). Resting B cells were obtained by magnetic cell

separation (MACS) using anti-CD43 beads (Miltenyi), as per manufacturer's instructions. Percentage of B1-8^{hi} cells was determined by flow cytometry after staining a cell aliquot with 5 μg/mL NP$_{19}$-PE (Biosearch Technologies).

To generate GCs, male C57BL/6 recipient mice were first primed intraperitoneally (i.p.) with 50 μg OVA absorbed in alum (Imject Alum, Thermo Scientific) at 2:1 v:v ratio in 100 μL volume, and then boosted two to four weeks later with 25 μg NP$_{(16)}$-OVA (Biosearch Technologies), delivered subcutaneously (s.c.) into the hind footpad. One day prior to boosting, B1-8^{hi} B cells of the indicated genotypes were adoptively transferred at the proportions depicted in each figure. Where indicated, 6 days after immunization with NP-OVA, 5 μg of DEC-OVA, produced in our laboratory as described (Pasqual et al., 2015), was injected s.c. into the hind footpad. In the experiments described in Figure 1 (B, E, F) Ly75$^{-/-}$ mice were used as recipients, to control for the presence of DEC-205 on host cells. In this case, to prevent the rejection of Ly75-expressing cells that is observed in a fraction of Ly75$^{-/-}$ host mice approximately one week after adoptive transfer, Ly75$^{-/-}$ hosts were further crossed to a transgenic line expressing human DEC-205 (which does not bind DEC-OVA) under the CD11c promoter (LY75-tg) (Kamphorst et al., 2010). We do not observe rejection of Ly75$^{+/+}$ cells in these hosts (our unpublished data), presumably due to tolerization of the immune system to mouse DEC-205 due to presence of the human ortholog. Our results using wild-type or Ly75$^{-/-}$LY75-tg hosts across multiple experiments are undistinguishable [compare, for example, (Victora et al., 2010) and (Bannard et al., 2016)]; we therefore used wild-type hosts for most experiments. For titration of the dose of DEC-OVA (Figures 1G and 1H), mice were injected with either 5 μg/footpad of DEC-OVA or 1 μg of DEC-OVA supplemented with 4 μg of anti DEC-205 antibody fused to the irrelevant antigen P. falciparum circumsporozoite protein (DEC-CS) (Boscardin et al., 2006), which is required to achieve a quantitative decrease in OVA targeting to DEC205-expressing cells (Gitlin et al., 2014). For CD40L blockade experiments (Figures 1I and 1J), mice were injected intravenously (i.v.) with 200 μg of a CD40L blocking antibody (Clone MR-1, BioXCell) or 200 μg of Armenian Hamster IgG isotype control (BioXCell) 2 hr prior to injection of DEC-OVA.

Rapamycin was purchased from LC Laboratories and diluted at 10 mg/mL in ethanol. Prior to injection, the stock solution was further diluted in PBS and injected i.p. at 2.5 mg/kg at the indicated time points. For CD40 activation experiments (Fig.S1E-F), mice were immunized with 10 μg/footpad of keyhole limpet hemocyanin (KLH, Sigma) absorbed in alum, and, after 10 days, anti-CD40 agonist antibody (Clone FGK4.5, BioXCell) was injected s.c. at 25 μg/footpad. To generate polyclonal GCs, mice were immunized s.c. with NP$_{(19)}$-KLH in alum at 2:1 ratio. Skin-draining lymph nodes were harvested 14 days later. For ELISA experiments, mice were immunized i.p. with 50 μg of NP$_{(16)}$-OVA absorbed in alum. For sequencing of primary GCs shown in Figure 7, mice were immunized s.c. with 10 μg/footpad of NP$_{(16)}$-OVA absorbed in alum.

Flow Cytometry and Cell Sorting

Popliteal lymph nodes were harvested, macerated in PBE, and filtered through a 70 μm mesh. Single-cell suspensions were incubated for 5 min with 1 μg/mL of anti-CD16/32 (24G2, eBioscience) and then stained on ice for 30 min in PBE using the reagents listed in the Key Resources Table. Cells were maintained at 4°C at all times until acquisition. For phospho-S6 staining, incubation was precisely timed to prevent time-related variations in dephosphorylation by endogenous phosphatases. Fixation/Permeabilization [Cytofix/Cytoperm (BD)] following cell-surface staining was timed to happen exactly 30 min after euthanasia for each sample. This was followed by staining with anti-phospho-S6 diluted in Perm/Wash buffer for 2 hr. For cell cycle analysis or staining of dsRNA content, fixed and permeabilized cells were stained in Perm/Wash buffer with 10 μg/mL Hoechst (Invitrogen) for 5 min or 4 μg/mL Pyronin Y (Sigma). Samples were acquired on Becton Dickinson Fortessa or LSR-II flow cytometers. For Foxo1 staining, nuclear permeabilization was performed per manufacturer instructions using the Foxp3 Staining Buffer Set (eBioscience) after prior fixation of surface-stained samples in paraformaldehyde 2% for 10 min. To detect glucose uptake in vivo, 5 mg/kg of 2-(N-(7-nitrobenz-2-oxa-1,3-diazol-4-yl)amino)-2-deoxyglucose (2-NBDG) was injected i.v. 25 min prior to lymph node harvesting. Detection of cells in the early S phase of the cell cycle was performed using dual nucleotide pulse, as described elsewhere (Gitlin et al., 2014). Briefly, mice were injected i.v. with 1 mg of 5-ethynyl-2'-deoxyuridine (EdU) and one hour later with 2 mg of 5-bromo-2'-deoxyuridine (BrdU). Lymph nodes were harvested 30 min after the second injection. Nucleotide incorporation into DNA was assayed with Click-iT Plus EdU Alexa Fluor 647 Flow Cytometry Assay Kit (Invitrogen) and FITC BrdU Flow Kit (BD). Cells in early S phase were defined as BrdU$^+$EdU$^-$. Unless otherwise indicated, GC cells were gated as live/singlet cells, CD19$^+$, Fas^{hi}, and CD38$^-$. For cell sorting, cells were stained as above and index-sorted directly into plates containing guanidine thiocyanate buffer (QIAGEN) supplemented with 1% β-mercaptoethanol using a FACS Aria II (BD). Data were analyzed in Flowjo v.8.7 and v.10.0.8. Extraction of single cell Forward Scatter values from LZ and DZ gates was performed using the ImmPortFCSConvLogicleTrans tool in GenePattern (Broad Institute).

Immunofluorescence

Lymph nodes were harvested and immediately fixed at 4°C in PBS containing 4% paraformaldehyde and 10% sucrose for 1 hr, followed by overnight incubation at 4°C in a solution of 30% sucrose in PBS. Tissues were embedded in optimum cutting temperature compound and cut into 20 μm sections using a Leica Cryostat Microtome. Sections were fixed in pre-cooled acetone at −20°C for 10 min, and blocked with Streptavidin/Biotin Blocking Kit (Vector Laboratories). Samples were stained in four steps: (1) rat anti-AID; (2) goat anti-rat Alexa 555; (3) rat anti-CD35 biotin and rabbit anti-c-Myc; and (4) streptavidin BV421, anti-rabbit Alexa 488 and anti-phospho-S6 Alexa 647. The antibodies used are described in Key Resources Table. Incubations were performed in PBS containing 5% BSA, 10% normal mouse serum and 0.1% Triton X-114. Sections were mounted in Fluoromount-G (SouthernBiotech) and imaged on a Zeiss 700 confocal microscope using a 20 × objective with numerical aperture of 0.8.

RNA Sequencing

Each sample consisted of 200-500 cells sorted from individual mice. Data shown in Figures 1 and S1are derived from 3 independent biological replicates. Both $Ly75^{+/+}$ and $Ly75^{-/-}$ cells were sorted from the same mice 12 hr after DEC-OVA injection, totaling 6 paired samples from 3 mice. Data in Figure S3 are from 4 independent biological replicates. Untreated $Ly75^{+/+}$ and $Ly75^{-/-}$ cells were sorted from the same mice, and rapamycin-treated $Ly75^{+/+}$ cells were from different mice, totaling 12 samples (4 $Ly75^{+/+}/Ly75^{-/-}$ untreated pairs and 4 $Ly75^{+/+}$ treated samples). Rapamycin was given at the time of DEC-OVA injection and cells were sorted 24 hr after DEC-OVA. Cells were sorted directly into guanidine thiocyanate buffer (QIAGEN) supplemented with 1% β-mercaptoethanol followed by RNA isolation using Agencourt RNAClean XP Beads (Beckman Coulter). RNA was then reversely transcribed into cDNA using an oligo(dT) primer and amplified as described (Trombetta et al., 2014). Nextera XT was used to prepare a multiplexed pooled library of fragmented and uniquely indexed samples for each flow-sorted population. Sequencing was performed on an Illumina HiSeq 2500 at the Whitehead Institute Genome Technology Core. For analysis, 40-bp single-end reads were pseudo-aligned using Kallisto version 0.43.0 against mouse transcriptome (Ensembl GRCm38 - release 79). Gene expression was inferred from transcript expression levels using the tximport R package as transcripts per million reads (TPM). Enrichment analysis was performed using GSEA software v2.2.3 (Broad Institute), with the following settings: 1000 gene set permutations; data collapsed to gene symbols using max_probe mode; enrichment statistic = weighted; ranking metric = signal2noise. 1 was added to all TPM values to reduce noise from transcripts with very low abundance.

Photoactivation

12 hr prior to imaging, mice bearing photoactivatable B1-8^{hi} GCs received adoptive transfer of 5×10^6 naive B cells expressing CFP and were injected i.v. with Texas Red-conjugated CD35 antibody. For photoactivation, mice were anesthetized with 1.5% isoflurane, and popliteal lymph nodes were surgically exposed as described previously (Victora et al., 2010). GC DZ were located as areas adjacent to CD35-expressing FDCs and devoid of CFP$^+$ naive B cells, photoactivated in vivo by scanning with a multiphoton laser tuned to 850 nm wavelength, and then imaged at 940 nm wavelength. Laser power conditions for photoactivation differed slightly according to each GC. To ensure that cell viability was maintained after photoactivation, the motility of PAGFP-transgenic cells was checked immediately after in vivo photoactivation. After photoactivation, either mice were sacrificed immediately (for control lymph-nodes) or incisions were sutured and mice were held for 8h and then sacrificed. All imaging experiments were carried out using an Olympus BX61WI upright microscope (Olympus 25X 1.05 NA Plan water-immersion objective), fitted with a Mai-Tai DeepSee Ti-Sapphire laser (Spectraphysics).

Generation of Mtor^{F2108L} Mice

Mice were generated by CRISPR/Cas9 gene targeting. Cytoplasmic injection of Cas9 mRNA, chimeric sgRNA, and repair oligo into fertilized C57BL6 zygotes at the one-cell stage, as described (Wang et al., 2013; Yang et al., 2013(a)). Chimeric sgRNA was in vitro transcribed from a synthetic dsDNA template (gBlock, Integrated DNA Technologies) using the MEGAshortscript T7 Transcription Kit (Thermo Fisher Scientific) and purified using Ampure XP beads (Beckman coulter). The repair oligo was synthesized as an ssDNA ultramer, PAGE-purified (Integrated DNA Technologies). *Cas9* mRNA was purchased from Sigma-Aldrich.

Sequences used were as follows:

dsDNA template for chimeric sgRNA transcription (protospacer sequence in capital letters):

cgctgttaatacgactcactataggGATCTCAAAGCAGCTACCCCgttttagagctagaaatagcaagttaaaataaggctagtccgttatcaacttgaaaaagtggcaccgagtcggtgctttt

Repair oligo (differences from original C57BL6 sequence are in uppercase; mutations upstream of the AflII site were for use with a different sgRNA, and were not incorporated into the resulting mouse strain):

tatggccgagatttaatggaggcacaagaatggtgtcgaaagtacatgaagtcggggaacgtcaaAgaTctGacgcaGgcctgggacctctactatcacgtCttAagacggatctcTaagcaActGccGcaggtaggctctcgaggcatcctgggttcatctgtgcatccagactcgcttctgctggagacttatagaaa

Assessment of Rapamycin Resistance

For in vitro experiments, tail fibroblasts were obtained by cutting 1 cm tail tip from adult mice, and after a quick rinse in 70% ethanol, samples were cut into small pieces with a razor blade, followed by incubation in 1000U collagenase type II (GIBCO) overnight. The digestion product was filtered through a 100μm mesh and plated in DMEM with 20% FBS plus antibiotics and fungicides. Rapamycin was added to full DMEM at 0.1 nM to 100 nM. For in vivo determination of rapamycin resistance, mice were fasted overnight, then given 2.5 mg/kg of rapamycin i.p. or left untreated, and 30 min later, refed with normal mouse chow ad libitum for 45 min, and then euthanized for organ harvesting. Tissues were harvested and immediately snap-frozen in dry ice.

Immunoblotting

Frozen samples were lysed in ice-cold lysis buffer (50 mM HEPES (pH 7.4), 40 mM NaCl, 2 mM EDTA, 1.5 mM sodium orthovanadate, 50 mM NaF, 10 mM pyrophosphate, 10 mM glycerophosphate and 1% Triton X-100, and one tablet of EDTA-free complete protease inhibitors (Roche) per 25 mL. Cell lysates were cleared by centrifugation at 15,000 g for 10 min. Proteins extracts were denatured by the addition of sample buffer, boiled for 5 min, resolved by SDS–polyacrylamide gel electrophoresis and analyzed by immunoblotting.

Fetal Liver and Bone Marrow Chimeras

WT recipient mice were lethally irradiated with 900 Rads. Fetuses were harvested on days 13-16 of pregnancy. Livers were excised and macerated using a 70 μm cell strainer in sterile PBS supplemented with 0.5% BSA and 2 mM EDTA (PBE). 1-10 $\times$ 10^7 total fetal liver cells were transferred into irradiated recipients, which were then held for at least 8 weeks to allow hematopoietic reconstitution. Septra antibiotics were provided in drinking water for the first 8 weeks after reconstitution. Bone marrow chimeras were generated using a similar protocol, except that hematopoietic cells were harvested from femurs and tibiae by flushing with PBE.

ELISA

High-affinity and total NP-specific antibodies were measured by ELISA using 10 μg/ml of $NP_{(2)}$-BSA or $NP_{(24)}$-BSA as the coating reagent, respectively. Serum was assayed in 3-fold dilutions starting at 1/100. NP-specific IgG_1 was detected using goat anti–mouse IgG_1 Fc-specific antibody conjugated to horseradish peroxidase and developed with tetramethylbenzidine (Sigma). OD450 was measured using a VERSAmax microplate reader (Molecular Devices). Titers were calculated by logarithmic interpolation of the dilutions with readings immediately above and immediately below an OD450 of 0.2 (for example, if OD450 readings at dilution 2 (1/900) = 0.3 and at dilution 3 (1/2700) = 0.1, then Titer = dilution = 2.5 = 1/1558.

Assessment of VH Mutations

Single GC B cells were sorted, RNA was isolated and cDNA was transcribed as described for RNA-seq. VH186.2 genes were sequenced and the number of total mutations per cell, including the W33L mutation conferring high affinity for NP (Allen et al., 1988) was determined. Sequences from B1-8[i] cells were distinguished from endogenous cells bearing the same or similar rearrangements based on the silent T>C mutation present in codon 92 of B1-8[i] but not in wild-type VH186.2 (Sonoda et al., 1997), which was not included in the SHM count.

QUANTIFICATION AND STATISTICAL ANALYSIS

The exact values of n indicating the total number of animals per group, as well as the definition of center, dispersion and precision measures are reported in each figure and figure legend. In Figures 1, 2, and 4–6, individual values for each animal are plotted and bars represent the mean of each group. In Figure 3D, individual values for each cell are plotted and bars represent the mean of each germinal center. In Figure 3E, the mean of each germinal center from a different mouse is plotted. In Figure 7, the mean of each group of mice ± SEM is shown. Student t test or χ^2 test with Yates correction were performed as depicted in the Figures. Asterisks indicate statistical significance (* $p < 0.05$; ** $p < 0.01$; *** $p < 0.001$; **** $p < 0.0001$; n.s. non-significant). Analyses were carried out using Prism software v. 7.0 (GraphPad).

DATA AND SOFTWARE AVAILABILITY

Data Resources

Raw and processed data files for the RNA sequencing analysis have been deposited in the NCBI Gene Expression Omnibus under accession number GEO: GSE98778.